Remote Sensing of Environment 268 (2022) 112789

Contents lists available at ScienceDirect

Remote Sensing of Environment

journal homepage: www.elsevier.com/locate/rse

The influence of surface canopy water on the relationship between L-band backscatter and biophysical variables in agricultural monitoring

S. Khabbazan [a,*], S.C. Steele-Dunne [b], P. Vermunt [a], J. Judge [c], M. Vreugdenhil [d], G. Gao [a]

[a] Department of Water Resources, Faculty of Civil Engineering and Geosciences, Delft University of Technology (TU Delft), Stevinweg 1, Delft 2628 CN, South Holland, Netherlands
[b] Department of Geoscience and Remote Sensing, Faculty of Civil Engineering and Geosciences, Delft University of Technology (TU Delft), Stevinweg 1, Delft 2628 CN, South Holland, Netherlands
[c] Center for Remote Sensing, Department of Agricultural and Biological Engineering, University of Florida, Gainesville FL 32611, USA
[d] Department of Geodesy and Geoinformation, Vienna University of Technology (TU Wien), 1040 Vienna, Austria

ARTICLE INFO

Edited by Jing M. Chen

Keywords:
Dew
Interception
Radar
Crop monitoring
Vegetation optical depth (VOD)
Cross ratio

ABSTRACT

The presence of surface water on the canopy affects radar backscatter. However, its influence on the relationship between radar backscatter and crop biophysical parameters has not been investigated. The aim of this study was to quantify the influence of surface canopy water (SCW) on the relationship between L-band radar backscatter and biophysical variables of interest in agricultural monitoring. In this study, we investigated the effect of SCW on the relationship between co- and cross-polarized radar backscatter, cross ratios (VH/VV and HV/HH), and radar vegetation index (RVI) and dry biomass, vegetation water content (VWC), plant height and leaf area index (LAI). In addition, the effect of SCW on estimated vegetation optical depth (VOD) and its relationship with internal VWC was investigated. The analysis was based on data collected during a field experiment in Florida, USA in 2018. A corn field was scanned with a truck-mounted, fully polarimetric, L-band radar along with continuous monitoring of SCW (dew, interception) and soil moisture every 15 min for 58 days. In addition, pre-dawn destructive sampling was conducted to measure internal vegetation water content and dry biomass. Results showed that the presence of SCW can increase the radar backscatter up to 2 dB and this effect was lower for cross ratios (CRs) and RVI. The Spearman's rank correlations between radar observables and biophysical parameters were, on average, 0.2 higher for dry vegetation compared to wet vegetation. The estimated VOD from wet vegetation was generally higher than those from dry vegetation, which led to different fitting parameter (so-called *b*) values in the linear fit between VOD and VWC. The results presented here underscore the importance of considering the influence of SCW on the retrieval of biophysical variables of interest in agricultural monitoring. In particular, they highlight the importance of overpass time, and the impact that daily patterns in dew and interception can have on the retrieval of biophysical variables of interest.

1. Introduction

Quantification of crop biophysical parameters is essential for many applications including agricultural management, yield forecasting, crop health monitoring and soil moisture estimation. Providing continuous and reliable crop information enables farmers and food producers to implement timely interventions to maximize yields and make optimal use of resources. Satellite data are increasingly used to estimate crop biophysical parameters such as leaf area index (LAI) (Brakke et al., 1981; Jiao et al., 2009; Gao et al., 2013; Hosseini et al., 2015; Chang, 2020), crop height (Fieuzal et al., 2012; Gao et al., 2013; Liao et al., 2018), dry biomass (Brakke et al., 1981; Ferrazzoli et al., 1992; Paloscia and Pampaloni, 1992; Gao et al., 2013; Chang, 2020) and vvegetation water content (VWC) (Saatchi et al., 1995; Steele-Dunne et al., 2017; Kim et al., 2018). LAI is related to crop productivity and growth (Kross et al., 2015) and is a vital input parameter for crop growth and yield forecasting models (Jiao et al., 2009; Molijn et al., 2014). Crop height and dry biomass are also important indicators for crop development (Liao et al., 2018), crop identification and crop yield estimation (McNairn and Brisco, 2004). VWC can provide information to support irrigation management (Dzikiti et al., 2010; Thenkabail and Lyon, 2016) and drought assessment (Tucker, 1980; Penuelas et al., 1993), and is an

* Corresponding author.
E-mail address: s.khabbazan@tudelft.nl (S. Khabbazan).

https://doi.org/10.1016/j.rse.2021.112789
Received 25 June 2021; Received in revised form 14 October 2021; Accepted 29 October 2021
Available online 10 November 2021

essential parameter in soil moisture retrieval (Attema and Ulaby, 1978; Bindlish and Barros, 2001; Barrett et al., 2009). Vegetation optical depth (VOD) is increasingly used for vegetation monitoring in agricultural applications and natural ecosystems (El Hajj et al., 2019; Konings et al., 2019; Frappart et al., 2020).

Low frequency (1–10 GHz) radar data are not affected by atmospheric conditions, can penetrate clouds and can acquire data during day and night. Radar observations are sensitive to dielectric and geometric properties of crops such as vegetation water content, leaf size, stem density, as well as the moisture and roughness of the underlying soil. Furthermore, microwaves penetrate the canopy, with lower frequencies penetrating deeper into the canopy and the underlying soil. As a result, radar data are well suited to monitor soil and vegetation in agricultural applications (McNairn and Brisco, 2004; Steele-Dunne et al., 2017). Many ground-based experiments and campaigns based on airborne and satellite data have demonstrated the value of low frequency radar data in agricultural applications such as crop monitoring and classification, soil moisture estimation, and extracting bio- and geo-physical parameters from radar data (Brisco et al., 1998; McNairn and Brisco, 2004; Steele-Dunne et al., 2017). Several studies have investigated the sensitivity of radar backscatter to biophysical parameters of crops (e.g. (Inoue et al., 2002; Jiao et al., 2009; Jia et al., 2013)). Others have shown that L-band backscatter coefficients and RVI are highly correlated with VWC (Kim et al., 2011, 2013a; Srivastava et al., 2015; Ma et al., 2017), LAI (Kim et al., 2008; Jiao et al., 2010; Hosseini et al., 2015) and the fresh weight of various crops (Kim et al., 2008, 2013a). The launch of ESA's Sentinel-1 mission in 2014 and Radarsat Constellation Mission (RCM) in 2019 provide high temporal resolution SAR data with revisit time of 6–12 days and 4 days respectively. This unprecedented revisit time has accelerated the use of radar observation for monitoring temporal variability in agricultural areas (Han et al., 2017; Veloso et al., 2017; Vreugdenhil et al., 2018; El Hajj et al., 2018, 2019; Kumar et al., 2018; Khabbazan et al., 2019; Mahdianpari et al., 2019; Ouaadi et al., 2020; Mandal et al., 2020a). However, little attention has been paid to the potentially confounding influence of surface canopy water (SCW) on retrieval of crop biophysical parameters. The SCW is generally referred to the presence of water in a form of dew or interception on the canopy surface.

Dew is often present on vegetation in temperate regions during the early morning (Hornbuckle et al., 2006; Kabela et al., 2009). Kabela et al. (2009) found that dew was present on more than 80% of days during the SMEX-05 experiment in Ames, Iowa, with dew accumulating on corn and soybean fields between 00:30 and 6:30 Central Standard Time (CST). As most satellites carrying radar instruments are in a near-polar, sun-synchronous orbit with local overpass times between 4:00 AM/PM and 10:00 AM/PM, the effect of dew on the radar signal needs to be considered. Several early experimental studies have reported an increase in radar backscatter at different frequencies due to the presence of SCW caused by dew and interception. Allen and Ulaby (1984) sprayed water to simulate rainfall on the canopy and found that the presence of water on canopies can increase X-band backscatter from wheat, soybean and corn by up to 2–3 dB. The dynamic range in VV-pol backscatter for the look angle of 50 degree for wheat, corn and sorghum during the whole season was around 7.59, 6.02 and 6.28 dB respectively. Gillespie et al. (1990) used a truck-mounted scatterometer in a wheat field to show that dew produced an increase of 1 dB in L- and Ku-band backscatter and 4 dB in C-band. Herold et al. (2001) and Riedel et al. (2002) investigated the effect of dew and interception on fully polarimetric X-, C-, and L-band data acquired by an airborne E-SAR system over different crop types, including corn. Among these three bands, the strongest influence of dew and interception was found at the cross-polarized L-band, while at the X-band and L-VV no significant influence of dew on radar backscatter was observed. They found that the influence of dew on the radar backscatter was independent of crop type. Wood et al. (2002) found that the presence of dew during descending (dawn) acquisitions of RADARSAT-1 resulted in values which were 2.5 dB higher than those from the ascending (dusk) acquisitions. In a recent controlled experiment, Brancato et al. (2017) explored the influence of SCW on differential interferometric observables using a multifrequency (S-, C-, X-, and Ku-band), fully-polarimetric scatterometer. They found that the influence of SCW on the interferometric coherence was comparable to that due to changes in soil or plant water status. They also reported dependence between the interferometric observables and change in plant surface moisture in X- and Ku-bands. Moreover, in S- and C-band they observed a more noticeable effect in VV polarization especially for canopies with a vertical orientation such as maize. These studies provide valuable insight into the potential impact of SCW on radar observables, but are limited to temporally sparse data.

A recent field study by Vermunt et al. (2020) combined sub-daily L-band radar data from a truck-mounted scatterometer with continuous observations of leaf surface wetness, surface and root zone soil moisture, and dense destructive vegetation sampling over an entire growing season of corn. The daily cycle of dew accumulation and dissipation, and the interception of precipitation and irrigation events, were shown to result in sub-daily variations in L-band backscatter. Vermunt et al. (2020) highlighted the potentially confounding influence of the SCW on the retrieval of biophysical parameters.

The aim of this study was to quantify the influence of SCW on the relationship between radar observables and geophysical variables. The analysis was based on L-band data collected in an intensive field campaign during an entire growing season of corn. L-band data are particularly relevant in the context of the future availability of L-band SAR data from NISAR (Rosen et al., 2017) and ROSE-L (Pierdicca et al., 2019). In this study, first the effect of SCW on different radar observables such as co- and cross-polarization data (σ_{VV}, σ_{HH}, σ_{XP}), polarimetric ratio data (σ_{VH}/σ_{VV} and σ_{HV}/σ_{HH}), and Radar Vegetation Index (RVI) was investigated. Then, correlation analyses were conducted between these radar observables and dry biomass, Vegetation Water Content (VWC), plant height and Leaf Area Index (LAI) at different growth stages of the corn plant. Finally, vegetation optical depth (VOD) was estimated in each polarization, and the effect of SCW on VOD estimation from L-band radar data was investigated.

2. Data and methods

2.1. Field experiment

2.1.1. Study area

This study was conducted at the University of Florida Institute of Food and Agricultural Sciences (UF/IFAS) Plant Science Research and Education Unit (PSREU) near Citra, Florida, USA (29.4° N, 82.17° W). The site is classified as *Cfa* under the Köppen Geiger Climate classification, described as a humid subtropical climate with hot and humid summers, and cold to mild winters (Peel et al., 2007). The rainy season runs from around May to November (Black, 1993). The corn field was 250 m by 150 m and the soil had >90% by volume fine sand (Bongiovanni et al., 2015). Sweet corn *(Zea mays L. var. rugosa)* was planted on 13 April at a row spacing of 92.5 cm with an average density of 7.9 plant m^{-2}, and harvested on June 18 before the start of the senescence stage. Center-pivot irrigation was applied throughout the season as needed. It was generally applied late in the evening, and was frequently needed during the dry period in the early season.

2.1.2. Hydrometeorology

The presence and duration of SCW, such as dew and interception, was monitored using Phytos31 dielectric leaf wetness sensors. These sensors closely approximate the thermodynamic and radiative properties of a leaf. Moreover, the surface of the sensors are hydrophobic, similar to the hydrophobic cuticle of a corn leaf. A sensor detects the presence of water on its surface by measuring its dielectric constant, which is highly sensitive to water. The sensor output threshold for 'water on the sensor' is based on factory calibration (METER Group, 2021) and

regularly checked by visual inspection. Three sensors were installed outside the radar footprint, at different heights in the canopy. The sensors were evenly distributed along the height of the plants, and their positions were adjusted as the plant height increased. Precipitation and irrigation data were used to classify the SCW as precipitation, irrigation or dew.

Meteorological data were obtained from the nearby weather station from the Florida Automated Weather Network (FAWN). The station was located <600 m from the experimental site. 15-min observations of rainfall, relative humidity, temperature, solar radiation and wind speed were obtained from the Report Generator (https://fawn.ifas.ufl.edu/data/reports/). The timing and amount of irrigation was provided by UF/IFAS. Soil moisture was observed using Decagon EC-5 sensors (METER Group, 2021a) installed at 5, 10, 20, 40 and 80 cm depth in two pits adjacent to the radar footprint. Data were collected every 15 minutes. Prior to installation, a site-specific calibration was performed in the laboratory using soil samples from the field. The goodness of fit for the linear regression between soil moisture estimates from the EC-5 sensors and values from gravimetric sampling was 0.993, and the RMSE was 0.028 m^3m^{-3}. Although the two profiles were 40 m apart, the observations of the two pits closely matched, and their average was used in this study.

2.1.3. Ground vegetation sampling

Predawn destructive vegetation sampling was conducted every 2–3 days during the entire growing season to measure VWC and dry biomass (m_d). Four rectangular sampling areas with average dimensions of 30 by 35 m^2 were delineated outside, but adjacent, to the radar footprint at the beginning of season. For each sampling event, eight field-representative plants were chosen from the four sampling areas. From the eight samples, all constituents (leaves, stems, ears, tassel and tillers) of these plants were separated, paper towel-dried, weighed, and oven dried at 60° C for 5 to 7 days. The dry samples were weighed again to estimate field-average VWC and m_d as follows (Vermunt et al., 2020):

$$\mathrm{VWC} = (W_f - W_d) \times \rho_{\mathrm{plant}} \tag{1}$$

$$m_d = W_d \times \rho_{\mathrm{plant}} \tag{2}$$

where W_f and W_d are the average fresh and dry weight of the eight samples (kg) respectively and the ρ_{plant} is the average number of plants per square meter (m^{-2}). The samples were also used to estimate field-average plant height using measuring tapes. Weekly detailed vegetation geometry data were used to determine Leaf Area Index (LAI) on seven dates during the growing season. Leaf length and width were measured, and used to estimate the leaf area, which was summed per plant and subsequently multiplied by plant density to obtain LAI. Visual identification of growth stages was performed on sampling days, using the *Biologische Bundesanstalt, Bundessortenamt and Chemical industry* (BBCH) scale for corn (Meier et al., 2009).

2.2. Radar data

Radar backscatter was measured using the truck-mounted University of Florida L-band Automated Radar System (UF-LARS) (Nagarajan et al., 2013) (Table 1). Radar data were acquired at four polarization combinations (VV, HH, VH, and HV) using a dual polarization horn antenna. The VH and HV data were very similar so, following previous studies (Liu et al., 2016), they were averaged and are referred to here as the cross-polarized backscatter σ_{XP}. The system was installed on a Genie platform with an antenna height of 14 meter from the soil surface. UF-LARS scanned the corn field with a fixed elevation angle of 40°. In this study, samples at three azimuth scans at −9°, 0° and +9° were used. At each azimuth scan, nine samples were taken at 30 MHz increments from 1130 to 1370 MHz which resulted in 27 independents samples. Individual samples are prone to noise due to fading, i.e. the noise arising from interference between returns from multiple ground targets (Bush and Ulaby, 1975). The average of 27 samples were used in order to account for variations in row direction, and to increase the signal-to-noise ratio, which for a single sample is lowered by fading (Liu et al., 2016).

Table 1
UF-LARS system specifications.

Parameter		UF_LARS
Frequency (GHz)		1.25
3dB Beamwidth (deg)	E-Plane	14.7
	H-plane	19.7
Bandwidth (MHz)		300
Antenna type		Dual-polarization horn
Range resolution (m)	HH/VV/XP	8.5/6.2/6.2
Azimuth resolution (m)	HH/VV/XP	4.7/6.4/4.7
NEσ° (dB)	HH/VV/XP	−23.43/−25.58/−48.12
Error in σ° (dB)	Systematic	1.49
	Random	0.85
Incidence angle (deg)		40
Platform height (m)		14

Internal calibration was applied during each acquisition to account (among others) for the effect of temperature on the electronics. External calibration was conducted using a trihedral corner reflector of known radar cross section several times during the growing season. The Single Target Calibration Technique (STCT) (Sarabandi and Ulaby, 1990) was used to calculate the backscatter coefficient σ° from the received signal. The total systematic error and random error were estimated as 1.49 and 0.85 dB respectively (Nagarajan et al., 2013; Liu et al., 2016). The ground range and azimuth range for each polarization combination were determined using the 3 dB antenna beamwidth of 14.7° and 19.7° in E-plane and H-plane respectively as shown in Table 1. Scanning the corn field over 3 azimuth angles resulted in the total footprint area of 120, 119 and 87.5 m^2 in HH, VV and XP polarization respectively. Vegetation samples were collected outside, but adjacent, to the radar footprint to avoid introducing patches and heterogeneity within the radar footprint, and to prevent any changes in roughness due to foot traffic. All sensors and hardware are installed outside the footprint to avoid any influence of metal structures or cables on the radar backscatter. The UF-LARS system was programmed to automatically acquire 32 measurements per day during the growing season. During the last 7 days, this was reduced to 16 measurements per day to avoid any radio frequency interference with other microwave sensors.

3. Methodology

3.1. Radar data

In addition to analyzing the radar backscatter itself, time series of Radar Vegetation Index and Cross Ratio were also considered. The RVI is calculated using:

$$\mathrm{RVI} = \frac{8\sigma_{\mathrm{VH}}}{\sigma_{\mathrm{HH}} + \sigma_{\mathrm{VV}} + 2\sigma_{\mathrm{VH}}} \tag{3}$$

where σ_{HH}, σ_{VV} and σ_{VH} are the observed linear backscatter intensities [–]. Here, σ_{XP} which is the average of σ_{VH} and σ_{HV} is used instead of σ_{VH}. The RVI was first introduced by Kim and van Zyl (2009) and is often used to monitor vegetation growth (Kim et al., 2011, 2013b; Mandal et al., 2020a,b), map vegetation cover (Haldar et al., 2020; Mandal et al., 2020b), and monitor crop development (Kim et al., 2011; Huang et al., 2016). RVI is a (dimensionless) normalized index that ideally varies between zero (bare soil) and one (Szigarski et al., 2018).

The cross ratios CR_H and CR_V are defined as σ_{XP}/σ_{HH} and σ_{XP}/σ_{VV} in the linear domain respectively (Vreugdenhil et al., 2018). Recall that the average of σ_{VH} and σ_{HV} is used as the cross-polarized backscatter (σ_{XP}) here. Hence, the only difference between the CR_H and CR_V here is in the

denominator. CRs and RVI are less sensitive to surface soil moisture variations (Veloso et al., 2017; Vreugdenhil et al., 2018; Khabbazan et al., 2019) and are considered useful indicators of crop growth (Jiao et al., 2009; Kim et al., 2011; Veloso et al., 2017; Vreugdenhil et al., 2018; Khabbazan et al., 2019).

The influence of SCW on radar observables was quantified by comparing radar observations from early morning (6 AM) to the first observations after SCW had dissipated. Generally this occurred at around 10 AM. Spearman's rank correlation coefficient (ρ) was used to quantify the effect of SCW on the relationship between six radar observables and four plant biophysical parameters.

3.2. Vegetation Optical Depth (VOD) estimation

The VOD estimation approach is based on that of Vreugdenhil et al. (2016), where the VOD can be estimated from the decrease in sensitivity of backscatter over bare soils as a result of vegetation. Fig. 1 shows an illustrative time series of backscatter in a vegetated area. The upper and lower limits of the backscatter time series are referred to as the wet reference (σ^0_{wet}) and dry reference (σ^0_{dry}) respectively. The wet reference corresponds to the backscatter values one would obtain under saturated soil conditions. The dry reference at some time **t** ($\sigma^0_{dry}(t)$) is the value corresponding to backscatter from a completely dry soil. It is a combination of a static component ($\sigma^0_{s,dry}$ e.g. due to soil texture, roughness etc.) and a dynamic component due to vegetation phenology. Vegetation growth leads to an increase in the dry reference, which indicates that the change in backscatter in response to a given change of soil moisture is assumed to be less than that during the bare soil period (Wagner et al., 1999). Note that this implicitly assumes that any change in the sensitivity to soil moisture is entirely due to the change in attenuation, and neglects any changes in double bounce or multiple-scattering.

The vegetation optical depth (VOD) is a measure of the degree to which the vegetation attenuates backscatter from the soil, and is a parameter of the Water Cloud Model (Attema and Ulaby, 1978). Vreugdenhil et al. (2016) showed that the VOD can be expressed at any time step as the difference between the sensitivity of backscatter to soil moisture changes in bare soils and the observed sensitivity attenuated by the vegetation in terms of the dry and wet reference as follows:

$$\mathrm{VOD}(t) = \frac{-\cos\theta}{2}\ln\left(\frac{\sigma^0_{wet} - \sigma^0_{dry}(t)}{\sigma^0_{wet} - \sigma^0_{s,dry}}\right) \quad (4)$$

The value of σ^0_{wet} was determined by averaging the highest backscatter values observed during the soil moisture peaks throughout the season. Vreugdenhil et al. (2016) used the Integral Equation Method to model backscatter and, in particular, to estimate $\sigma^0_{s,dry}$. In this study, the tower-based measurements of radar backscatter are combined with in situ soil moisture data to estimate the dry reference. Following Wagner et al. (1999) and Attema and Ulaby (1978), it is assumed that for a given vegetation water content, radar backscatter and soil moisture are linearly related. VWC influences the slope of this linear relationship. Therefore, a linear fit is obtained for a dynamic window (1–3 days) during which it is assumed that VWC is relatively constant. The dry reference $\sigma^0_{dry}(t)$ varies in time due to vegetation growth, so it was obtained by fitting a linear model between backscatter and soil moisture during a moving window, and extrapolating to determine the backscatter that would corresponds to a completely dry soil. The static component of the dry reference ($\sigma^0_{s,dry}$) was estimated based on the backscatter data from 1 to 3 May. This corresponds to the period after planting (April 13) and during the formation of the first leaves (see Table 2). Estimating $\sigma^0_{s,dry}$ during this period, rather than the bare soil period directly after planting, ensures that the soil surface has been smoothed by several irrigation events (see Fig. 4(b) and (c)), and that the roughness controlling $\sigma^0_{s,dry}$ is as close as possible to roughness under the growing canopy. The length of the dynamic window for the estimation of $\sigma^0_{dry}(t)$ was obtained using a rule-based decision tree. The window should be as short as possible to minimize the variations in vegetation water content. However, it needs to be long enough to ensure that there is some variation in soil moisture (and backscatter), and that sufficient data are included to obtain a reasonable goodness of fit, defined here as $R^2 > 0.7$ and $P < 0.05$. The leaf wetness sensor data were used to distinguish between backscatter data obtained in the presence (wet) or absence (dry) of SCW due to dew or interception. The dry reference was determined separately for these two conditions. Hence, two time series of VOD were obtained. VOD_{dry} indicates the attenuation due to internal vegetation water content alone. It is the estimate of VOD obtained in the absence of any SCW. VOD_{wet} is the estimate of VOD based on observations obtained when SCW was present due to dew or interception.

Table 2
Description of BBCH codes and growth stages of sweet corn.

Period	Date	DAP	BBCH	Description
Early season	Apr 27	14	13	Leaf development - 3 leaves (V)
	May 11	28	21	Beginning of tiller formation (V)
Mid season	May 18	35	30	Beginning of stem elongation (V)
	May 23	40	51	Beginning of tassel emergence (V)
	May 28	45	55	Middle of tassel emergence (V)
Late season	Jun 1	49	63	Male: Beginning of pollen shedding (R) Female: tips of stigmata visible (R)
	Jun 8	56	69	End of flowering (R)
	Jun 13	61	73	Development of suit - Early milk (R)

V = Vegetative stage; R = Reproductive stage.

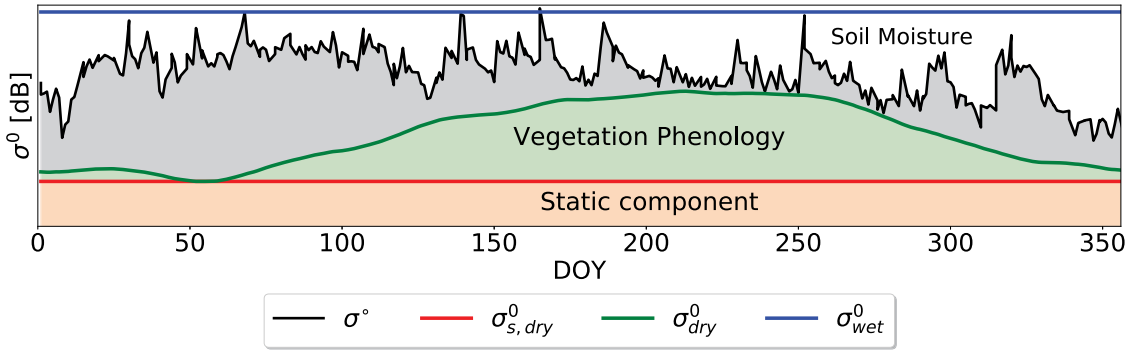

Fig. 1. Illustration of the wet reference (σ^0_{wet}), and static components ($\sigma^0_{s,dry}$) and dynamic components of the dry reference (σ^0_{dry}) as three components of the TU Wien soil moisture retrieval method along with radar backscatter coefficient (Steele-Dunne et al., 2019). (For interpretation of the references to color in this figure legend, the reader is referred to the web version of this article.)

4. Results

4.1. Hydrometeorological data

4.1.1. Weather data

Daily precipitation and irrigation and 15-minute air temperature, relative humidity, and solar radiation are presented in Fig. 2. The early season (26 April to 18 May) was hot and dry with strong daily cycles in air temperature and relative humidity. Irrigation was applied at midnight on 8 occasions to ensure moisture availability for plant growth. During the mid-season (19 May to 30 May), rainfall occurred on most days with three particularly heavy rainfall events on 21, 27 and 30 May. Nighttime temperatures were generally warmer than in the early season, so the amplitude of the daily temperature cycle was less than during the early season. The late-season was dry and warm with high temperatures and solar radiation and a few small rain events.

4.1.2. Root zone soil moisture

Fig. 3 shows the volumetric soil moisture (θ) at five depths. In general, soil moisture at 5 and 10 cm were highly affected by irrigation and precipitation events, while the soil moisture content was mostly stable at 20, 40, and 80 cm depth. The soil moisture at 80 cm depth was only affected by very heavy rainfall events. The effect of midnight irrigation during the early season can be seen as a rapid increase in 5 cm and 10 cm soil moisture, followed by a clear dry down. The soil moisture at 20 cm was slightly affected by irrigation events, but the water did not infiltrate to the sensors at 40 and 80 cm. During the mid-season, heavy rain events led to several abrupt increases throughout the root zone. Three intense rain events from 21 May to 1 June resulted in higher soil moisture content at 10 and 20 centimeters compared with soil moisture at 5 centimeters. The dry period from 2 June to 11 June resulted in a significant decrease in soil moisture at all depths. The minimum soil moisture observed in situ was 0.107 m^3 m^{-3}. This value will be considered as "dry soil" for the estimation of the dry reference.

4.1.3. Interception and dew data

Fig. 4 shows the presence and duration of water on the leaf wetness sensors at three different heights. Fig. 4(a), (b), and (c) shows results from the sensor installed at the upper, middle and lower canopy respectively.

During the early season, the canopy surface wetness was related to the presence of dew and midnight irrigation practices. During the mid-season, the surface of the canopy was mostly wet due to the frequent rain events. Fig. 4(d) shows the number of days on which SCW (dew or interception of precipitation/irrigation) was present as a function of time of day. Dew is almost always present from midnight until around 10 AM. The presence of SCW is 3.05 times more likely between 12 AM and 10 AM than between 11 AM and 11 PM.

4.2. Crop development

Data on crop development are shown in Fig. 5 and Table 2. While corn height continued to increase until the end of the season, the LAI reached its maximum value around 23 May. Slight variations in LAI are observed after this date due to variability within the field. However, leaf VWC (Fig. 5(a)) and leaf dry biomass (Fig. 5(b)) suggest that leaf

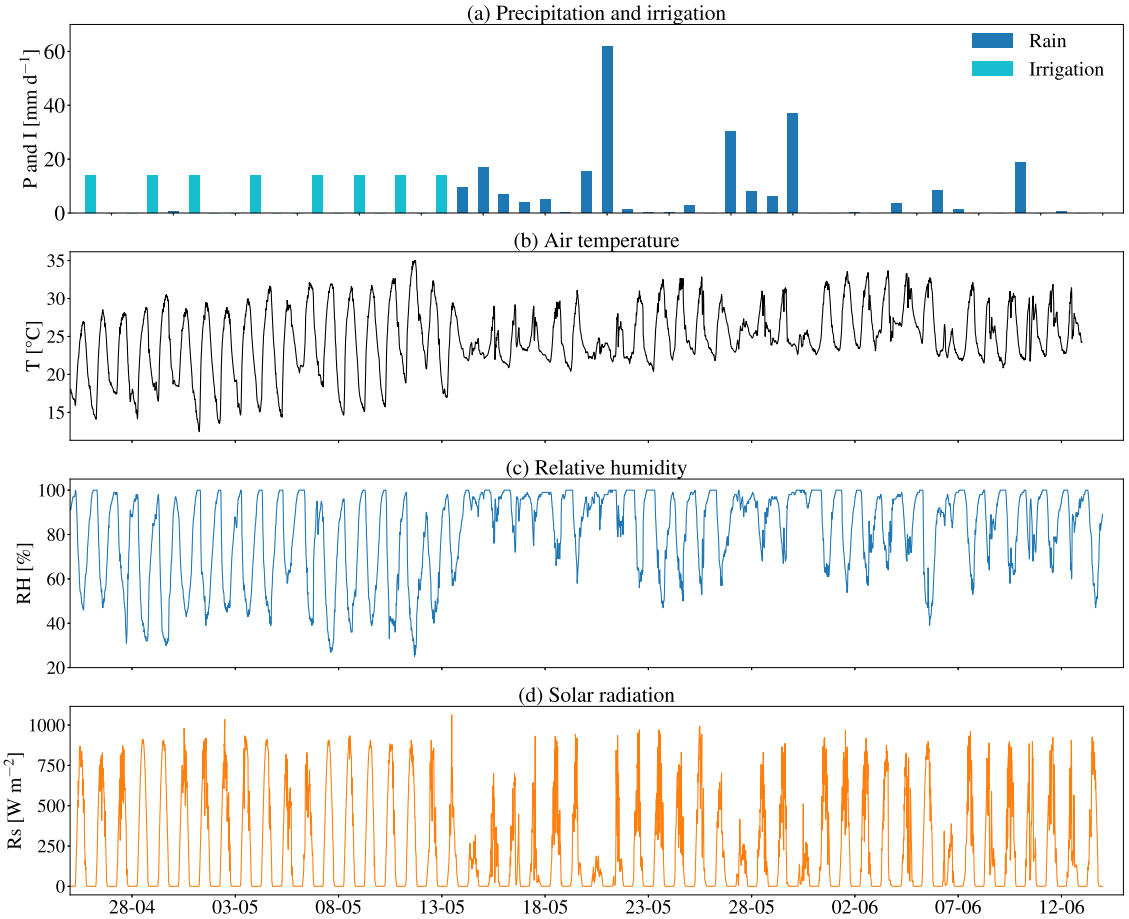

Fig. 2. Time series of meteorological data collected by Florida Automated Weather Network: (a) daily rainfall and irrigation (mm d^{-1}), (b) air Temperature at 2-meter height (°C), (c) relative humidity at 2-meter height (%) and d) solar radiation at 2-meter height (W m^{-2}).

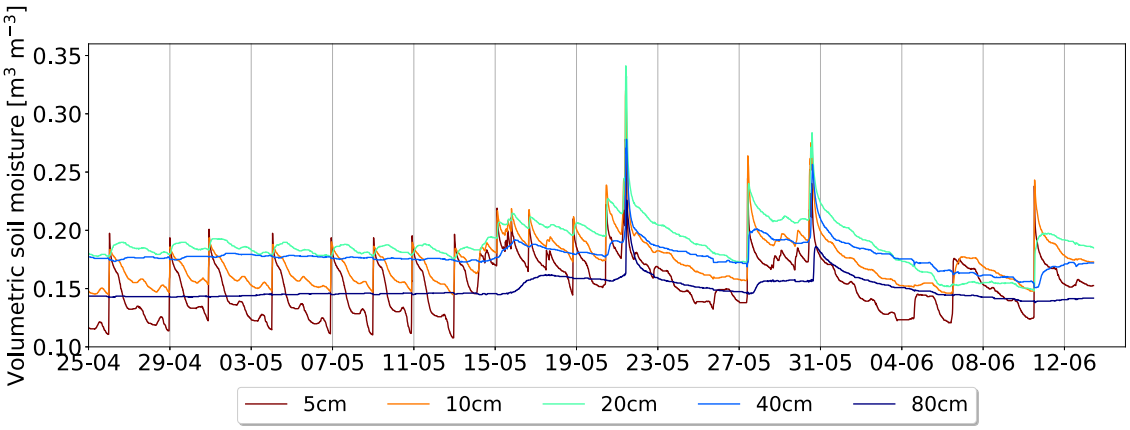

Fig. 3. Averaged volumetric soil moisture (m^3 m^{-3}) from two pits on different depths (5, 10, 40, and 80 cm). (For interpretation of the references to color in this figure legend, the reader is referred to the web version of this article.)

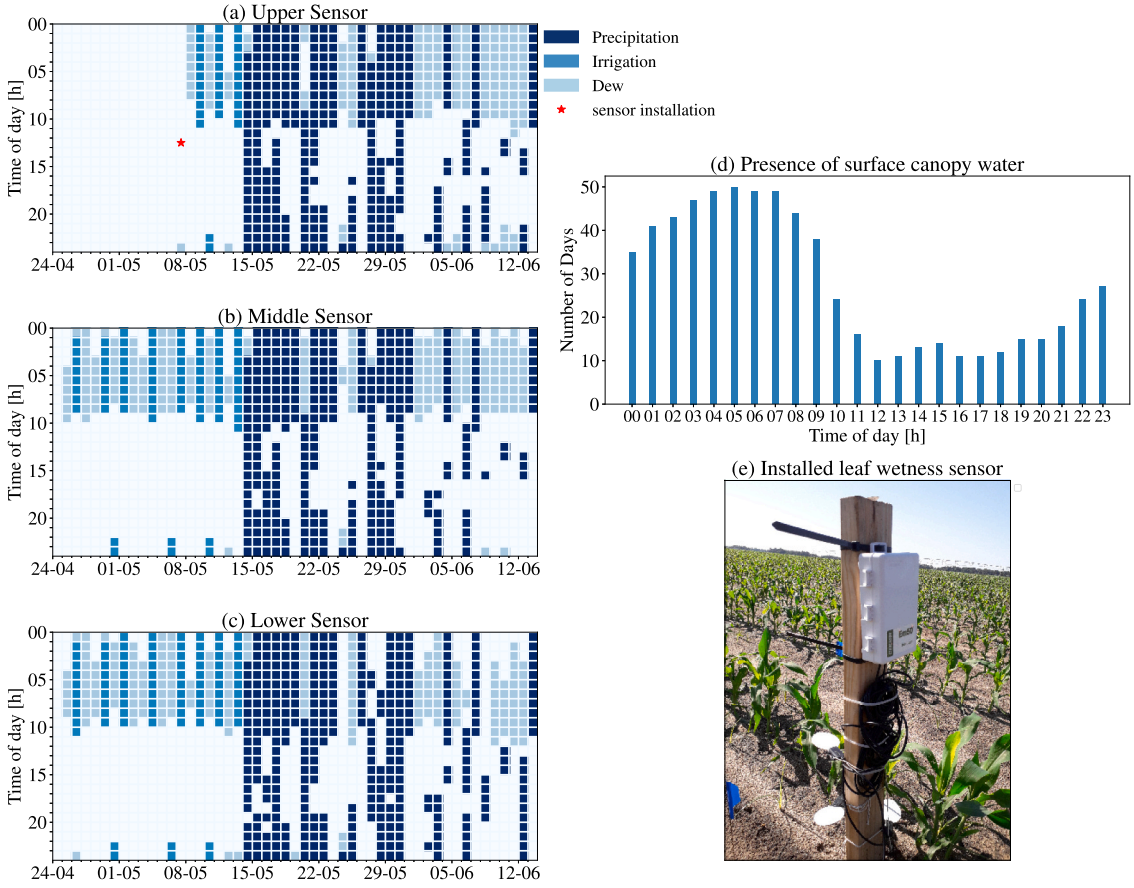

Fig. 4. Presence of SCW resulted from precipitation, irrigation, and dew on detected from (a) upper sensor, (b) middle sensor and (c) lower sensor. The red star on 7 May shows the installation date for the upper sensor. Colored squares represent detection of water in the sensors for at least 15 min during that hour. (d) The percent of days that SCW was presented at each hour of the day. (e) The picture of leaf wetness sensors at early stage. (For interpretation of the references to color in this figure legend, the reader is referred to the web version of this article.)

formation stabilized after this date. On 23 May, the dry biomass of both stems and leaves was almost equal but the stems account for 65% of the total VWC. The formation of corn ears at the start of June is clear from the increase in both dry biomass and ear water content. The stem VWC decreases by around 30% (−0.8 kg m^{-2}) from 1 to 8 June due to a combination of ear formation and separation, the decline in root zone soil moisture due to warm and dry weather conditions, and the start of senescence.

4.3. Time series of L-band backscatter and derived indices

Fig. 6(a) shows the seasonal variation in the observed radar backscatter. The increasing trend in backscatter during the early stage (27 April to 18 May) is due to crop growth. It is particularly clear in XP and VV, which are less sensitive than HH backscatter to soil moisture. Fluctuations of up to 5 dB are observed in all polarizations after irrigation events. The influence of biomass accumulation on backscatter

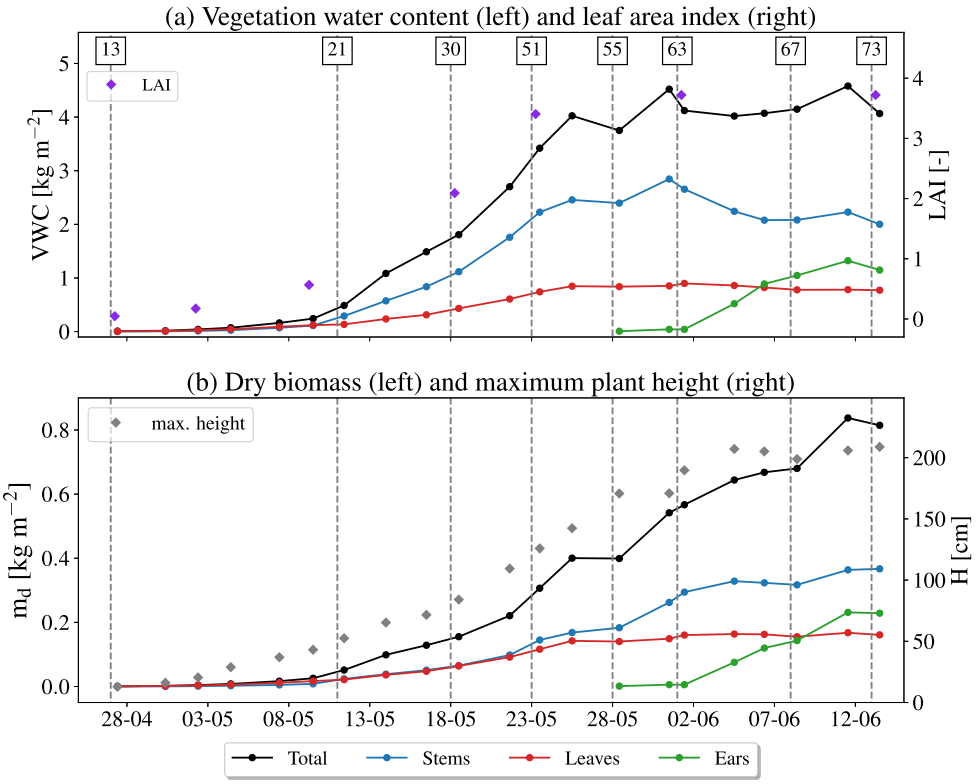

Fig. 5. Seasonal pattern of (a) vegetation water content (kg m^{-2}) per constituents and leaf area index, and (b) dry biomass (kg m^{-2}) per constituents and canopy height (cm). Phenological stages are shown by BBCH codes, which are explained in Table 2. (For interpretation of the references to color in this figure legend, the reader is referred to the web version of this article.)

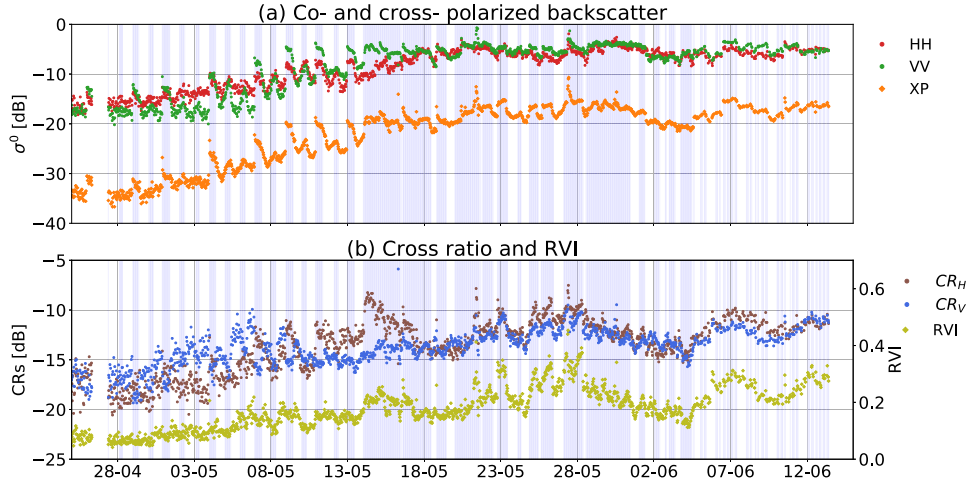

Fig. 6. Complete time series of L-band (a) HH, VV, and cross-polarized (XP) radar backscatter, and (b) CRs (CR_V, and CR_H) and Radar Vegetation Index (RVI). Light blue vertical lines indicate the presence of SCW during the radar acquisition. (For interpretation of the references to color in this figure legend, the reader is referred to the web version of this article.)

dynamics during the mid-season (19 – 31 May) is limited because the soil and vegetation are both wet for much of this period, resulting in persistently high backscatter. The lack of precipitation or irrigation from June 1 (Fig. 2) results in a drydown in the root zone (Fig. 3), and decrease in stem VWC (Fig. 5), which result in a decrease in cross-pol backscatter from −16 dB to −21 dB. Ear development from 2 to 12 June coincides with an overall increasing trend in XP- and VV-pol backscatter, with short-term variations corresponding to the precipitation events on 5 and 11 June.

In a previous study (Vermunt et al., 2020), the Tor Vergata Model (Bracaglia et al., 1995; Della Vecchia et al., 2006) was used to simulate the observed backscatter using the soil moisture and vegetation data discussed in Section 2.1. In addition to providing the total backscatter, the Tor Vergata model simulations also provide some insight into the relative importance of different scattering mechanisms to total backscatter and how this changes throughout the growing season. Direct scattering from the ground dominates co-polarized backscatter in the early season. Increasing biomass leads to attenuation of direct scattering

and increased double-bounce and multiple scattering between the vegetation and ground in both HH and VV. Direct scattering from vegetation dominates after mid-May, with double-bounce as the second largest contribution. This term is more significant in HH than VV and ensures some sensitivity to soil moisture throughout the growing season. In contrast, σ_{XP}° is dominated by direct vegetation scattering as soon as the vegetation emerges, with limited influence of soil moisture due to multiple scattering between the vegetation and ground.

In Fig. 6(b), CRs and RVI data clearly follow plant development, increasing steadily from 27 April to 28 May. The steady decrease in both CRs and RVI data from 28 May to 5 June coincides with the general decrease in stem VWC in response to high evaporative demand and decreasing root zone soil moisture availability (Fig. 2). The differences among the two CRs and RVI are greatest in the early season, i.e. before 18 May. The difference between the V-pol and H-pol CRs, in particular, can be attributed to the difference between HH and VV-pol backscatter during the early season due to the difference in their sensitivities to soil moisture and vegetation. The presence of system noise in the HH data partly explains higher variability in the CR_H at this time. The CR_V and CR_H converge after 18 May when backscatter is dominated by vegetation scattering. The divergence from 5 to 10 June may be attributed to the difference in sensitivity of VV and HH to changes in ear and stem VWC.

Fig. 7 shows the mean daily cycle of the radar backscatter for the period from June 1 to June 13. This specific period was chosen because the limited precipitation means that the SCW is primarily due to the presence of dew, and the corn has reached maximum biomass. There is clear daily cycle in radar backscatter in response to accumulation and dissipation of dew (shown in Fig. 4) and variations in internal water content (VWC). The maximum value is observed at the acquisition of 7:30 AM in VV and cross-pol, coinciding with the maximum dew accumulation. The minimum backscatter occurs in the late afternoon in all polarizations when the VWC reaches its minimum value. The increase in backscatter between 1:00 PM and 3:00 PM is due to the influence of rain events on 6 and 11 May. The range of the mean daily cycle in backscatter during this period is 0.78, 1.02, and 0.96 dB in HH, VV and cross-pol respectively. In Section 4.4, it will be shown that even larger variations are observed in the early and mid-season. A detailed discussion about the daily cycle of backscatter can be found in Vermunt et al. (2020).

4.4. Effect of surface canopy water on morning radar backscatter

Fig. 8 shows the difference in radar observables acquired during early and late morning, i.e. in the presence and absence of SCW. Dawson and Goldsmith (2018) found that the presence of SCW influenced cellular, leaf and whole-plant water relations through its role in suppressing transpiration and changing water potential. It is also assumed

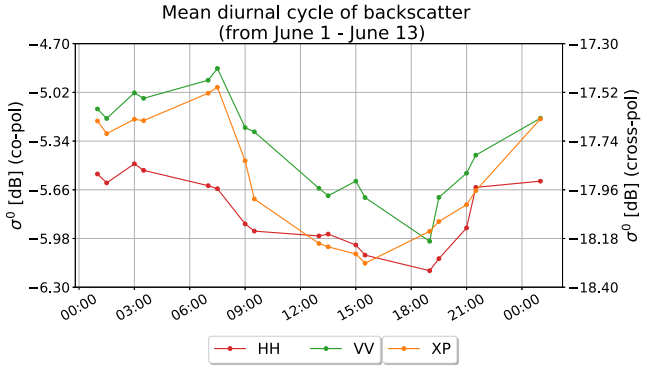

Fig. 7. Mean daily cycle of co- and cross-polarized backsactter for a 13 day period from June 1 to June 13. (For interpretation of the references to color in this figure legend, the reader is referred to the web version of this article.)

that the plant water potential has finished equilibrating with the soil by 6 AM and will not continue to rise during the mid-morning period (Slatyer and Markus, 1968). Therefore, it is assumed here that the presence of SCW limits transpiration, so that the change in internal water content between the 6 AM and late morning observations is limited.

Note from Fig. 8(a), that the coincident difference in soil moisture is less than 0.01 m^3m^{-3}, However, it is important to note that variations in backscatter in the early season may be affected by dew formation on the soil surface (Vermunt et al., 2020). The formation and dissipation of dew on the soil surface will not influence the observed 5 cm soil moisture, but will affect backscatter.

Fig. 8(a) shows that early morning backscatter is higher than late morning backscatter by up to 1.02 dB for co-pol and 1.27 dB for cross-pol, and can reach up to 3.56 dB (σ_{VV} on 9 May). Note that these differences are not negligible while the dynamic range for HH, VV and XP during the growing season was around 11.36, 8.19 and 12.93 dB respectively. The magnitude of the difference varies considerably during the growing season. Large differences, particularly in VV and XP are observed in the early season. However the low fractional cover during this period means that this is also influenced by dew on the soil. During the mid-season, the growing vegetation results in an increase in direct scattering from the vegetation and increased attenuation of the return from the soil. Note that large differences of up to 2.77 dB in XP (23th May), and 1.49 dB in HH and VV (25th May) occur on days when SCW was due to dew rather than interception. Differences of around 1 dB are observed in all polarizations in the late season with a maximum value of 1.37 dB observed in σ_{VV} on 11th June.

Fig. 8(b) shows the difference in early morning CRs and RVI due to the dissipation of SCW. On average, the difference between early- and late-morning CRs is 0.7 dB, and the average difference in RVI is 0.02. These are relatively small compared to the dynamic range of CRs and RVI observed in Fig. 6(b). However, the observed sensitivity of XP backscatter to SCW (Fig. 8(a)) means that both CRs and RVI are especially affected by SCW in the mid-season. Differences in this period are consistently positive, and reach up to 2 dB and 0.125 in CRs and RVI respectively.

4.5. VOD time series retrieved from dry and wet vegetation

Fig. 9 shows the dry reference, estimated separately for wet and dry vegetation. The annotation $\sigma^0_{\text{dry}-\text{PSCW}}$ and $\sigma^0_{\text{dry}-\text{ASCW}}$ indicates whether the dry reference was estimated from radar observations in the presence or absence of SCW. During the early season, sufficient data were available to estimate the dry reference for both wet and dry SCW conditions in VV and XP. Noise in the first few days of HH backscatter (Fig. 6(a)) resulted in goodness of fit values lower than our threshold for the linear fit between soil moisture and backscatter. Hence it was not possible to estimate $\sigma^0_{\text{dry}-\text{ASCW}}$ in HH reliably in the early season. Frequent rain events during the mid-season meant that there were not enough data to calculate $\sigma^0_{\text{dry}-\text{ASCW}}$ from 18 May to 1 June.

Both $\sigma^0_{\text{dry}-\text{PSCW}}$ and $\sigma^0_{\text{dry}-\text{ASCW}}$ increase during the vegetative stages as the fresh biomass increases. Recall that $\sigma^0_{\text{wet}} - \sigma^0_{\text{dry}}$ corresponds to the range within which backscatter varies due to soil moisture, and is therefore an indication of the sensitivity of backscatter to soil moisture. As σ^0_{wet} has a constant value for the growing season, an increase of σ^0_{dry} indicates a loss in sensitivity of backscatter to soil moisture as a result of vegetation attenuation. The rate of increase in σ^0_{dry} varies per polarization as backscatter in different polarizations is sensitive to different constituents of the canopy. The rapid increase in σ^0_{dry} in VV is due to stem elongation, while the more gradual increase in XP corresponds to the increase in LAI, which reaches a maximum around 23 May.

In general, $\sigma^0_{\text{dry}-\text{PSCW}}$ is higher than $\sigma^0_{\text{dry}-\text{ASCW}}$. In terms of Eq. (4), this means that the estimated attentuating effect of vegetation is higher in

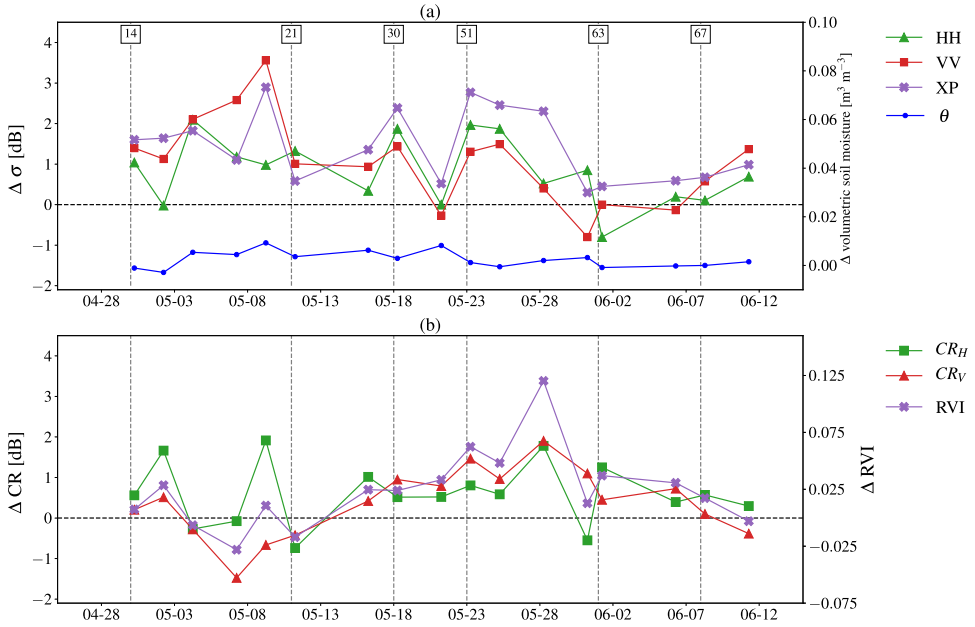

Fig. 8. Differences in early morning backscatter from wet and dry vegetation on destructive sampling dates. The difference is calculated between observations at 6 AM (wet vegetation) minus the first radar observation after the SCW has dissipated (10 AM–12 PM). Data are presented for (a) backscatter and soil moisture, and (b) CRs and RVI.

the presence of SCW. The difference between $\sigma^0_{\text{dry}-\text{PSCW}}$ and $\sigma^0_{\text{dry}-\text{ASCW}}$, depends on polarization, with a larger difference observed in VV than XP backscatter. In the absence of reliable data in the early season in HH, it is difficult to draw a conclusion about HH polarized data. In the late-season, drier weather ensured that sufficient data were available to estimate $\sigma^0_{\text{dry}-\text{PSCW}}$ and $\sigma^0_{\text{dry}-\text{ASCW}}$. In both VV and HH, $\sigma^0_{\text{dry}-\text{PSCW}}$ remains relatively flat in the late-season. Temporal variations in $\sigma^0_{\text{dry}-\text{ASCW}}$ vary with polarization. The increase in VV, for example, coincides with the increase in ear water content, while HH and XP are more sensitive to the leaf water content. Fig. 10 provides a closer view of the estimated wet and dry references in VV polarization during the early stages. While $\sigma^0_{\text{dry}-\text{ASCW}}$ increases relatively steadily during this period, $\sigma^0_{\text{dry}-\text{PSCW}}$ is influenced by irrigation events and dew formation. As dew accumulates, $\sigma^0_{\text{dry}-\text{PSCW}}$ increases, corresponding to a gradual reduction in sensitivity to soil moisture at 5 cm depth.

Fig. 11 shows the VOD for each polarization, estimated using Eq. (4). From 5 May onwards, the rapid increase in biomass of all plant constituents (Fig. 5) results in an increase in VOD. The rate at which it increases varies by polarization due to the sensitivity to different vegetation constituents. The sharpest increase is observed in VV due to the sensitivity to increasing biomass in the corn stems during the early stage.

Recall from Fig. 9 that $\sigma^0_{\text{dry}-\text{PSCW}}$ was always greater than $\sigma_{dry-ASCW}$. As a result, VOD values estimated in the presence of SCW are always higher than those estimated in its absence. The difference is particularly striking in the mid-season when interception following several heavy rainfall events results in significant variations in VOD in all polarizations. Fig. 4 showed the persistent presence of SCW in this period. As a result, few data were available to estimate $\sigma^0_{\text{dry}-\text{ASCW}}$ (Fig. 9) and hence VOD (Fig. 11) from dry vegetation during this period. Nonetheless, Fig. 11 shows that VOD in the presence of SCW reached up to 0.4–0.5, while that from dry vegetation was in the range 0.1–0.2. Three heavy rain events (Fig. 2) occurred on 21, 27, and 30 May. Their influence on the estimated VOD varies considerably with polarization due to the polarization-dependent sensitivity of backscatter to different constituents of the canopy (Fig. 9).

During the late-season (1–12 June), both VOD estimates in VV polarization increase steadily, coinciding with ear formation (Fig. 5). Between 1 and 8 June, the difference between VOD estimated in the presence and absence of SCW is around 0.1 for VV and HH, though barely any difference is discernible in XP.

4.6. *Effect of surface canopy water on the relation between radar backscatter data and crop biophysical variables*

Fig. 12 shows how each of the radar observables relates to the biophysical parameters of interest in the presence (blue) and absence (red) of SCW. The scatter plots and Spearman's rank correlation coefficient (ρ) values in Fig. 12 show that cross-polarized backscatter, and the indices derived from it, are strongly related to each of the biophysical parameters of interest. In general, ρ is consistently lower (by around 0.2) when the backscatter data are collected in the presence of SCW. This is true for all radar observables and all biophysical parameters. It is also clear that increase in backscatter due to SCW (Fig. 6) results in a different relationship between the radar observables and the biophysical variables, so the presence of SCW potentially has a confounding effect on the retrieval of biophysical parameters from radar observables. On the other hand, the dynamic range of backscatter values is marginally larger when backscatter is acquired in the presence of SCW. So, while the relationship may be less well-defined, there is greater sensitivity to the biophysical variables. This is clear, for example, in Fig. 12(m to p) where the sensitivity of the CR_V is higher for wet vegetation than for dry vegetation when BBCH < 55. The same is true in Fig. 12(u to x) for the RVI, particularly for BBCH < 55.

Recall from Fig. 5 that the rapid changes in biophysical parameters, particularly in VWC and LAI, occur before BBCH $= 55$. These rapid changes result in a strong increasing trend in backscatter, particularly in cross-polarization (Fig. 6). In contrast, after BBCH $= 55$, VWC is quite stable and the backscatter is closer to saturation. There is no increasing trend after BBCH $= 55$, but backscatter still varies in response to changes in the structure (e.g. ear formation), as well as changes in stem and ear VWC, their influence on the relative importance of different contributions to total backscatter. The domimant contribution to backscatter in all polarizations at this time is direct scattering from vegetation. So, the

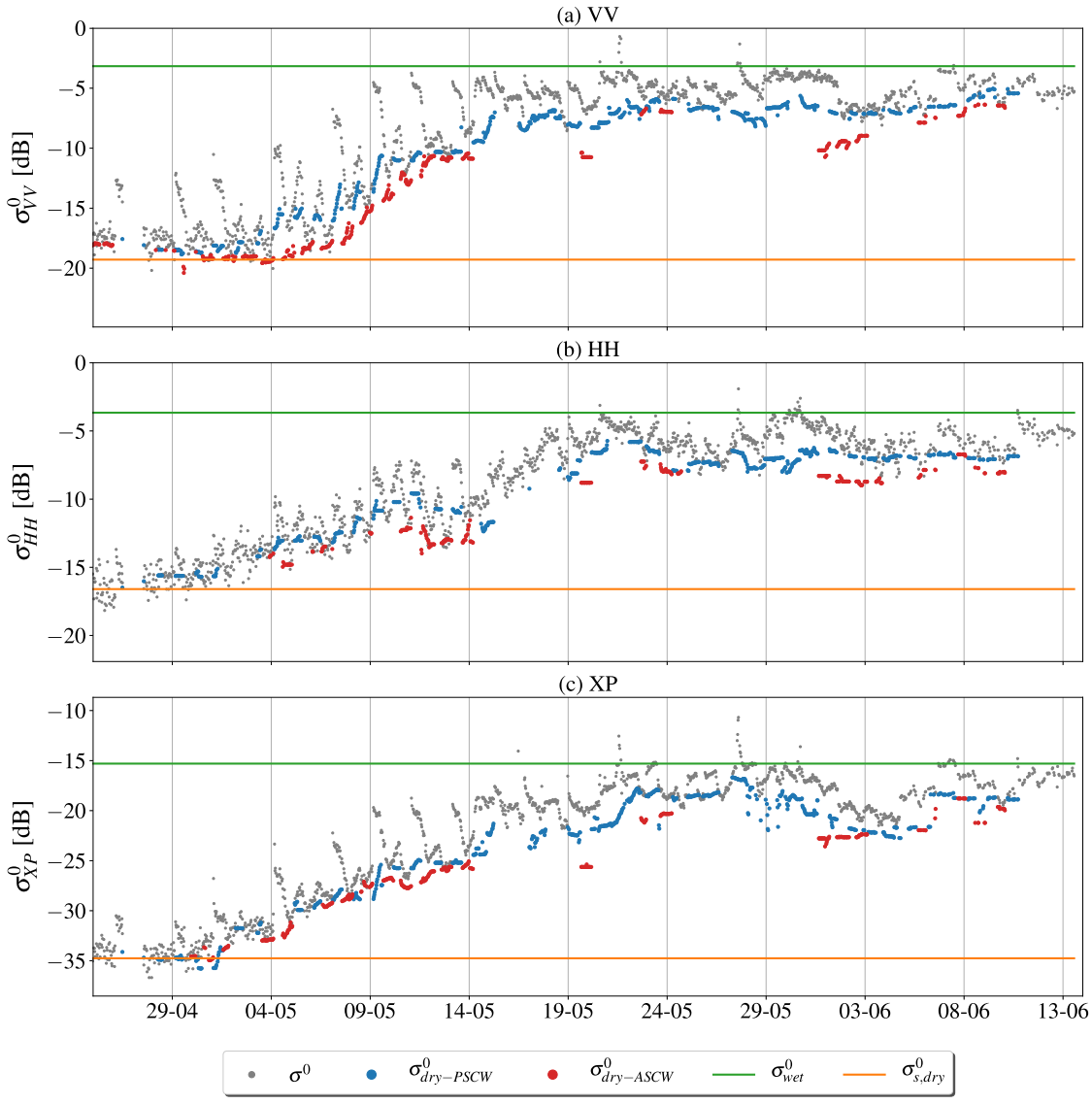

Fig. 9. Time series of radar backscatter along with the calculated static component ($\sigma^0_{s,\mathrm{dry}}$), the dry reference for wet vegetation ($\sigma^0_{\mathrm{dry-PSCW}}$) and dry vegetation ($\sigma^0_{\mathrm{dry-ASCW}}$), and the wet reference (σ^0_{wet}) for co- and cross-polarization data. The green and orange horizontal lines on each plot indicate the wet reference and the static component, both of which are constant for the entire growing season. (For interpretation of the references to color in this figure legend, the reader is referred to the web version of this article.)

variations are primarily due to vegetation, but some (limited) sensitivity to soil moisture remains due to the contribution of double-bounce. Consequently, the ability to relate biophysical parameters to radar observables is very different before and after BBCH = 55. This can also be observed in Fig. 12, where the relationship between the radar observables and biophysical parameters is not linear over the full range of biophysical parameter values.

Table 3 compares ρ between the radar observables and the biophysical parameters for ρ calculated using the whole season, or only the period before BBCH = 55. Due to the limited number of destructive sampling dates, note that this corresponding number of samples is 21 and 13 respectively. ρ values for which the corresponding P-vale is greater than 0.01 are indicated in bold in Table 3. For BBCH < 55, the presence of SCW leads to similar or higher ρ values when cross-polarized data are used (e.g. in XP, RVI and CR_V) and lower values of ρ when co-polarized data are used. When data from the whole season are used, ρ values are lower than those obtained using data for BBCH < 55 alone. The difference between the two is greater when the radar observables were acquired in the presence of SCW (i.e. "Wet").

4.7. *Effect of surface canopy water on relation between VOD and vegetation water content*

VOD is assumed to depend linearly on vegetation water content according to $VOD = b * VWC$. Fig. 13 shows the linear fit between VOD and total VWC for the whole season (a–c) and for the period with BBCH < 55. The goodness of fit (R^2) is up to 0.34 higher when the linear fit is limited to BBCH < 55 (Fig. 13d–e).

Recall from Fig. 5 that after BBCH = 55, the total VWC remains at around 4 kg m^{-2}, but the stem water content decreases and the ears form and separate from the stem. So, while VWC does not change, the internal moisture distribution changes and the canopy is undergoing structural changes which influence the backscatter (Fig. 6), and VOD (Fig. 10). Focusing on the relationship for BBCH < 55, the goodness of fit is > 0.94 for both VV and XP in the presence and absence of SCW. Values are lower for HH polarization, though this may be due to limited data. Goodness of fit values are similar in the presence and absence of SCW, so the assumption that there is a linear relationship is reasonable in both scenarios. Note, however, that VOD values obtained in the presence of

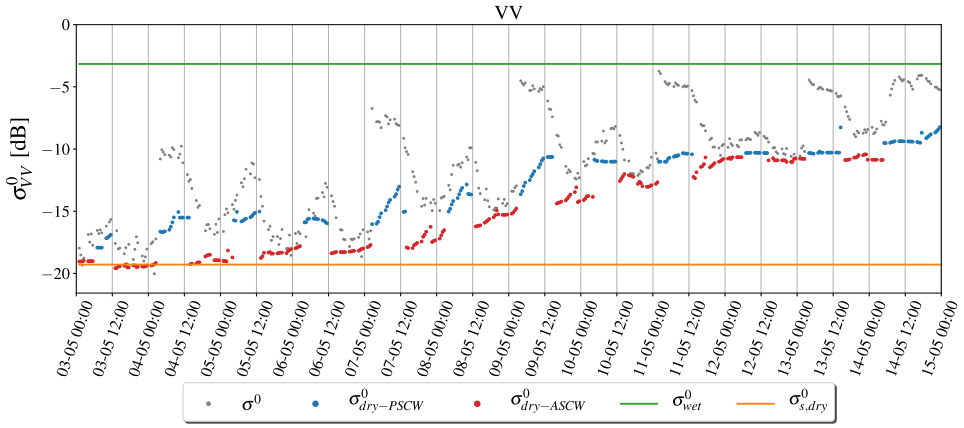

Fig. 10. Time series of radar backscatter along with the calculated static component ($\sigma^0_{s,\mathrm{dry}}$), the dry reference for wet vegetation ($\sigma^0_{\mathrm{dry-PSCW}}$) and dry vegetation ($\sigma^0_{\mathrm{dry-ASCW}}$), and the wet reference (σ^0_{wet}) for VV-pol and period of 3 to 15 May. (For interpretation of the references to color in this figure legend, the reader is referred to the web version of this article.)

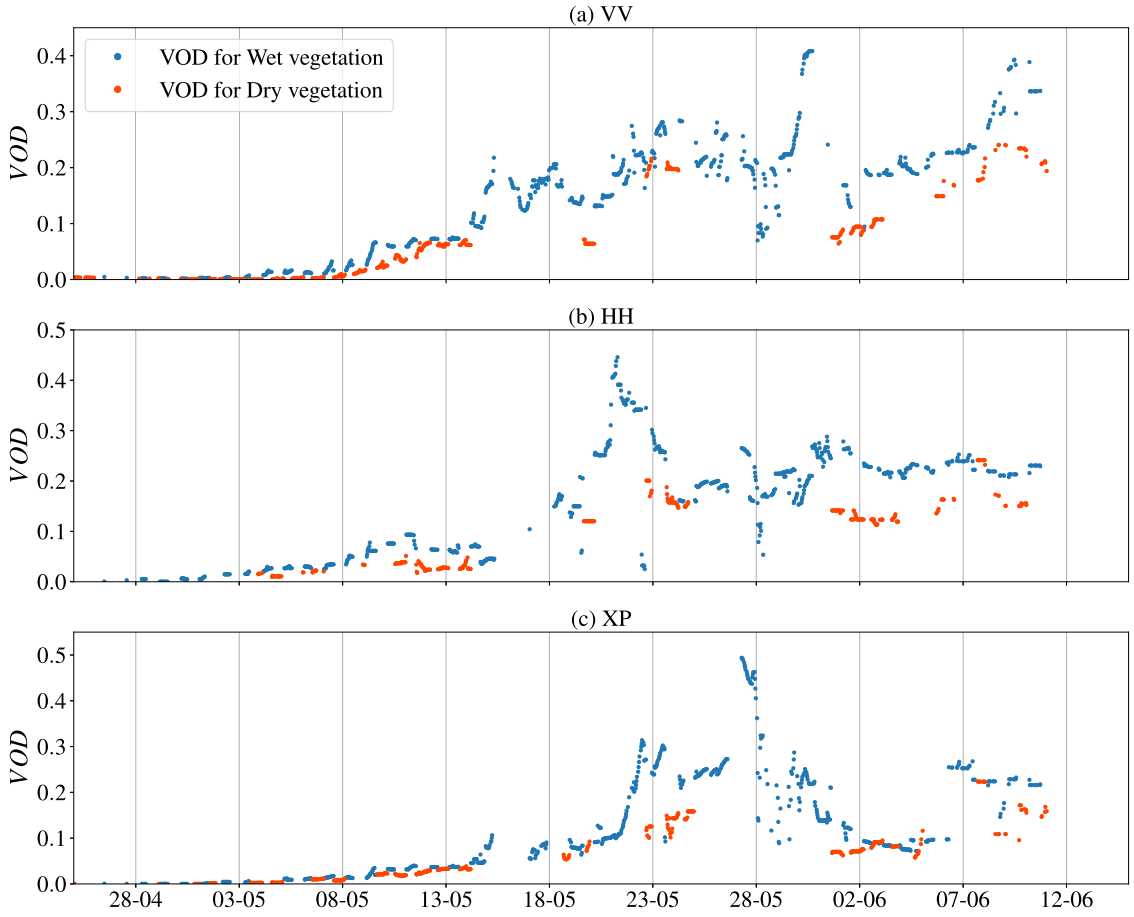

Fig. 11. Temporal pattern of VOD for wet and dry vegetation computed for (a) VV polarization, (b) HH polarization and (c) XP polarization. (For interpretation of the references to color in this figure legend, the reader is referred to the web version of this article.)

SCW (blue) are generally higher, than those obtained in its absence (red), and the difference increases with VWC. So, the linear regressions between VOD and VWC in the presence and absence of SCW are markedly different. The b parameters are generally much higher when estimated using VOD in the presence of SCW (Table 4). The difference occurs regardless of whether b is estimated using data from the entire season or the period where BBCH < 55.

5. Discussion

Results in Fig. 4 demonstrated that L-band backscatter is influenced by the presence of SCW, in the form of both dew and interception. This is

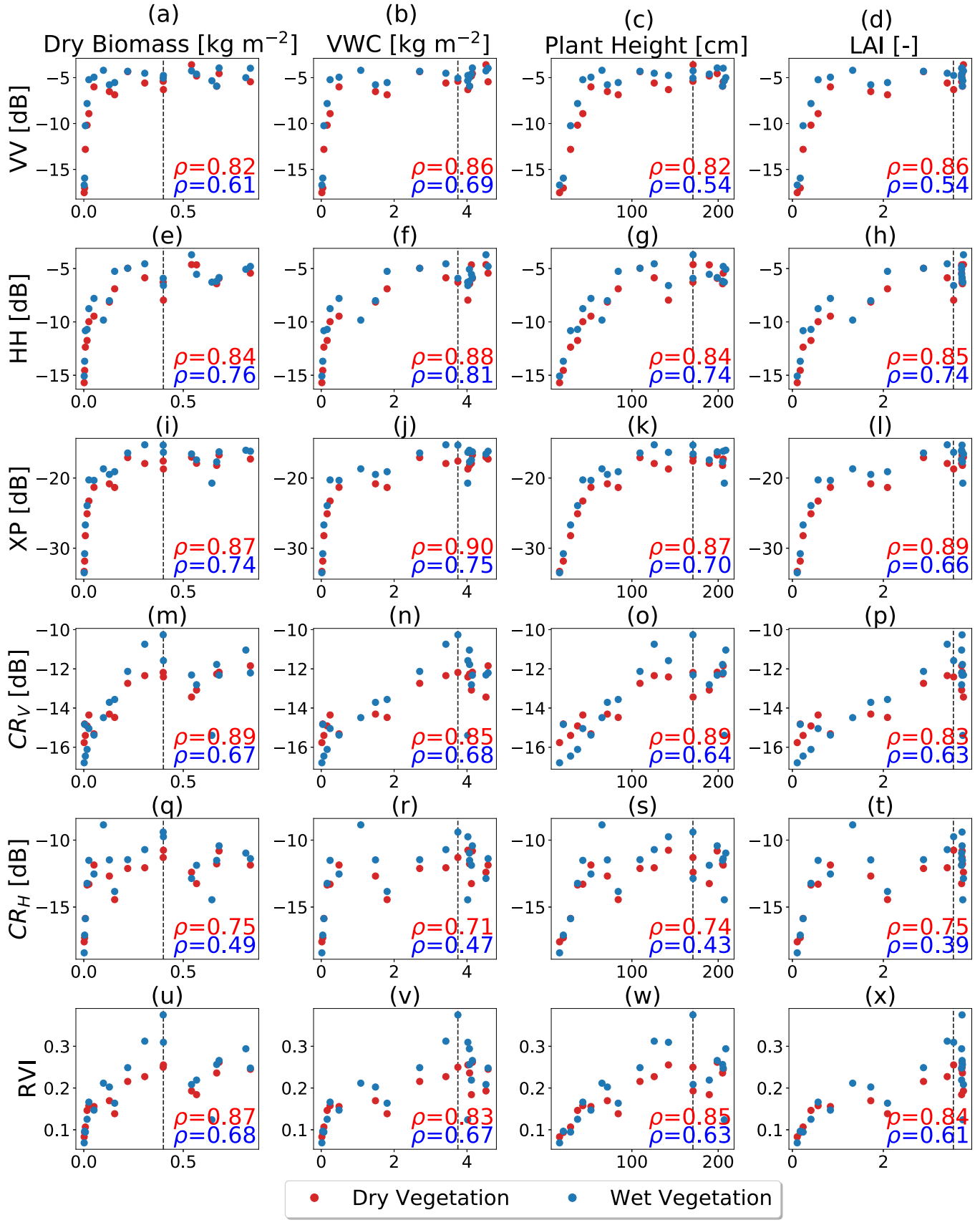

Fig. 12. The relationship between six radar observables and four key biophysical variables based on data from the full growing season. Blue and red indicate that the radar observables correspond to acquisitions from wet (including SCW) and dry (no SCW) vegetation. The corresponding Spearman's rank Correlation Coefficients (ρ) are in the lower right corner. The vertical dashed line indicates BBCH = 55 (middle of heading stages and start of ear formation). (For interpretation of the references to color in this figure legend, the reader is referred to the web version of this article.)

Table 3
Spearman's rank correlation coefficients between four biophysical variables and the six radar parameters for dry and wet vegetation at two different growing stages.

	Dry biomass				VWC				Plant height				LAI			
	BBCH < 55		Whole season		BBCH < 55		Whole season		BBCH < 55		Whole season		BBCH < 55		Whole season	
	Dry	Wet	Dry	Wet	Dry	Wet	Dry	Wet	Dry	Wet	Dry	Wet	Dry	Wet	Dry	Wet
VV	0.87	0.75	0.82	0.61	0.87	0.75	0.86	0.70	0.89	0.74	0.82	**0.54**	0.89	0.74	0.86	0.57
HH	0.90	0.89	0.84	0.76	0.90	0.89	0.86	0.80	0.92	0.89	0.84	0.74	0.92	0.89	0.85	0.74
XP	0.92	0.96	0.87	0.74	0.92	0.96	0.90	0.75	0.93	0.96	0.87	0.70	0.93	0.96	0.89	0.66
CRV	0.88	0.92	0.89	0.67	0.88	0.92	0.85	0.68	0.90	0.93	0.89	0.64	0.90	0.93	0.83	0.63
CRH	0.87	0.80	0.75	**0.49**	0.87	0.80	0.71	**0.47**	0.87	0.81	0.74	**0.44**	0.87	0.81	0.75	**0.39**
RVI	0.92	0.93	0.87	0.68	0.92	0.93	0.83	0.67	0.92	0.94	0.85	0.64	0.92	0.94	0.84	0.61

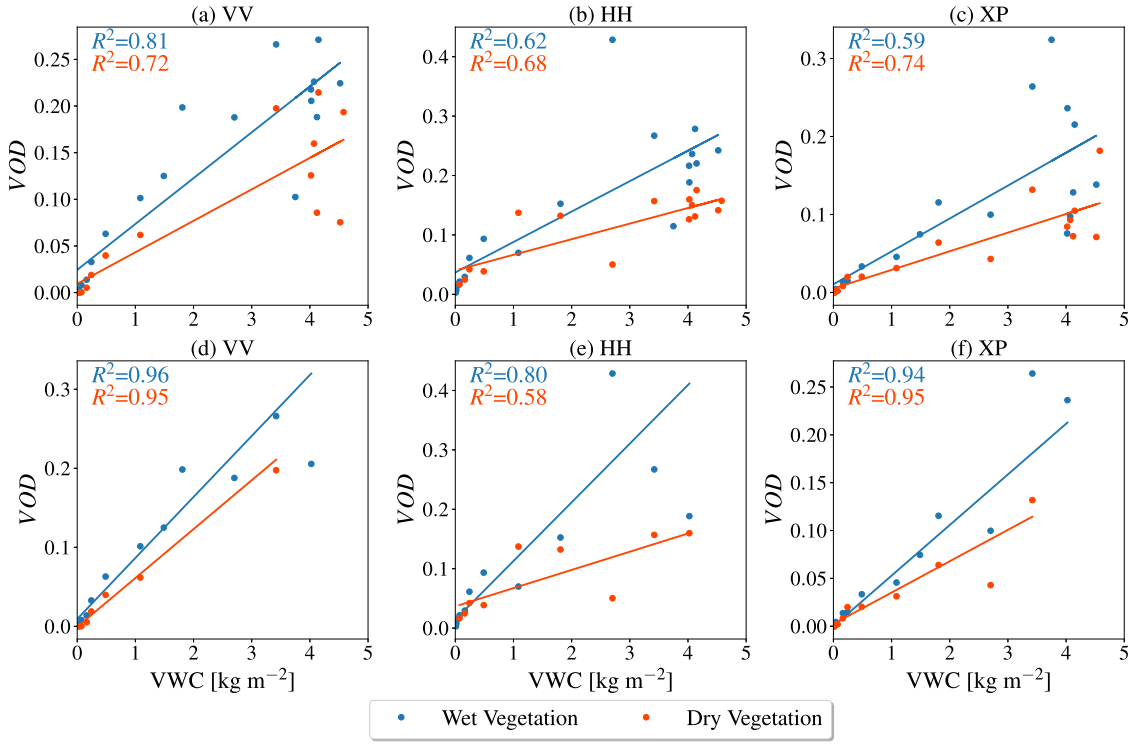

Fig. 13. Vegetation optical depth (VOD) calculated for VV- (left), HH- (middle) and cross-polarized backscatter (right), as a function of vegetation water content (VWC). Results are shown for the full growing season (a–c), and the period up to BBCH = 55 (d–f). The data, fitted linear regressions and goodness of fit (R^2) values are shown in blue and red to indicate if they were obtained in the presence (blue) or absence (red) of SCW. (For interpretation of the references to color in this figure legend, the reader is referred to the web version of this article.)

Table 4
Regression coefficient (*b*-factor) for each linear regression between VWC and VOD retrieved from VV, HH and XP backscatter.

Channel	BBCH < 55		Whole season	
	Dry	Wet	Dry	Wet
VV	0.06	0.08	0.03	0.05
HH	0.03	0.10	0.03	0.05
XP	0.03	0.05	0.02	0.04

compatible with previous studies (Gillespie et al., 1990; Hornbuckle et al., 2010; Sharma et al., 2020; Vermunt et al., 2020). Fig. 8 showed that the presence of early morning dew can contribute to a difference of up to 2 dB in L-band backscatter. This is consistent with previous studies (Wood et al., 2002; Hornbuckle et al., 2006; Vermunt et al., 2020; Sharma et al., 2020). However, here the availability of high temporal resolution data from both leaf wetness sensors and tower-based radar throughout the entire season allowed us to show that the impact of SCW on backscatter varies with growth stage and with polarization. In the early season, while the fractional cover was low, the difference between SCW and no-SCW conditions were large due to the combined influence of dew on the canopy as well as the soil. In the mid-season, the amount of SCW is higher due to both interception and dew, and the fact that LAI is much higher than the early-season. In the late-season, the LAI is still high, but the difference between SCW and no-SCW is lower than the early and mid-season because the high biomass means that radar backscatter is close to saturation and the SCW is almost entirely due to dew rather than a combination of dew and interception. It remains challenging to explain the differences observed between polarizations because there is a limited understanding of how the presence of droplets or a film of water affects the various contributions to total backscatter.

Unfortunatly, current models do not account for the presence of SCW (Ulaby et al., 1990; Bracaglia et al., 1995; Monsivais-Huertero and Judge, 2011; Monsivais-Huertero et al., 2018; Sharma et al., 2020).

In addition to backscatter, we also examined the influence of SCW on CRs and RVI. These are increasingly used to monitor vegetation because they are less influenced by soil moisture as they are normalized with co-polarized backscatter (Jiao et al., 2009; Kim et al., 2011; Veloso et al., 2017; Vreugdenhil et al., 2018; Khabbazan et al., 2019). The difference between early morning and late morning values, i.e. in the presence and absence of dew, was not zero. In fact, the difference in morning values during the mid-season was around a quarter of the dynamic range. This suggests that while CRs and RVI may be useful in mitigating the influence of soil moisture, they are not immune to the influence of SCW.

The relationships between radar observables (backscatter, CRs, RVI) and biophysical variables are most meaningful during the vegetative stages as they all monotonically increased in response to the accumulation of fresh biomass. This is consistent with previous studies (Jiao et al., 2009; Fieuzal et al., 2012; Jia et al., 2013; Hosseini et al., 2015; Huang et al., 2016). In the later stages the backscatter was closer to saturation, but it still varied in response to changes in the structure and internal distribution of moisture within and among constituents. This explains why the Spearman's rank correlation coefficient was lower when determined for the whole season rather than the stages where BBCH < 55.

Unlike previous studies, this study explicitly addressed the influence of time of day on the relationship between radar observables and biophysical parameters. Occasionally, rapid daytime growth can occur in the early vegetative stages when a dry spell ends. Generally though, LAI, dry biomass and plant height do not vary much on a single day. On the other hand, the impact of SCW on backscatter means that the timing of observations used to retrieve biophysical parameters matters. If we consider the entire growing season, results in Fig. 12 showed that the strength of the monotonic relationship between backscatter and the biophysical variables is higher (difference in ρ up to 0.25) when one uses backscatter collected in the absence of SCW. This is quite consistent with decades of research using destructive sampling of vegetation to prove that backscatter is sensitive to the dielectric constant of vegetation, which is primarily controlled by its water content. However, results in Table 3 showed that the lower ρ values were primarily due to the low sensitivity of backscatter to biophysical variables when BBCH > 55. During the vegetative stages, the ρ values were comparable in the presence and absence of SCW. Results for BBCH < 55 in Table 3 suggests that stronger relationships (higher ρ) were observed in the presence of SCW. This is consistent with the conclusions of earlier studies that argued that the presence of SCW made it easier to distinguish between crop types (Gillespie et al., 1990; Molijn et al., 2018). This is likely due to the influence of vegetation geometry on the amount of water that can be held by the vegetation.

However, it is essential to note that the relationship between the radar observable and the biophysical parameter is just different due to the higher values of backscatter obtained in the presence of SCW. If ground data are used to calibrate relationships between radar observables and biophysical parameters it is essential, therefore, to calibrate the relationship for the situation likely to be observed. For example, if early morning dew is common, and morning satellite overpasses will be used, these relationships need to be determined for wet vegetation.

VOD estimated using radar backscatter data obtained in the presence of SCW was generally higher than that obtained in its absence. This was true for all polarizations. The largest differences were found in the mid- to late-season, but the dynamics (i.e., the difference between VOD obtained in the presence and absence of SCW) were found to vary by polarization. This may be related to the polarization-dependent response of radar backscatter to SCW, but the influence of data scarcity cannot be overlooked.

VOD is often used as a proxy for vegetation water content as the two are assumed to be linearly related (Konings et al., 2019). However, results presented here show that the linear regression coefficient b is very different when the backscatter data are obtained in the presence and absence of SCW. Higher backscatter values in the presence of SCW result in considerably higher b values. It is important to highlight that VOD is not a biophysical parameter, but a parameter of an electromagnetic model, in this case the Water Cloud Model. The VOD is assumed to be a measure of the degree to which the signal from the soil is attenuated by the vegetation. However, the VOD time series contain artifacts from the manner in which VOD is estimated from this model and the validity of any inherent assumptions. For example, multiple scattering is not considered. This assumption is particularly problematic in the presence of SCW as any enhancement of multiple scattering due the presence of droplets or a film of water on the leaves is not accounted for. In addition, the methodology involves fitting a relationship between backscatter and soil moisture within some time window. The length of this window must be long enough to ensure a reasonable fit, but this implies that the dry reference (hence VOD) is constant within this window. Data sparsity and noise in the data will influence the VOD estimate, as will any rapid changes in VOD during the window due to growth or water uptake.

6. Conclusions

Data from an intensive field campaign were used to investigate the influence of SCW on the relationship between L-band backscatter and biophysical variables in crop monitoring. Continuous leaf wetness sensor data, combined with precipitation and irrigation data were used to chart the accumulation and dissipation of dew and interception throughout the growing season. These were combined with data from an L-band fully polarimetric tower-based radar to quantify the effect of SCW on L-band radar observables (backscatter, RVI and CRs), as well as the relationship between these observables and biophysical parameters of a corn crop. In addition, VOD was estimated to consider the effect of SCW on VOD, and its relationship with VWC.

At the study site in Florida, dew was present on the canopy for most days from 12 AM to 10 AM and was found to have a substantial effect on backscatter in all polarizations and throughout the growing season. The cross-ratio and RVI, often used to mitigate the influence of soil moisture, were not immune to the influence of dew and interception. Furthermore, it was shown that the presence of SCW affected the relationship between L-band observables and biophysical variables. This means that it is important to consider daily patterns in SCW and overpass time when deciding to retrieve biophysical parameters from radar data. Sentinel-1 and RCM are in near-polar, sun-synchronous orbits with local overpass times at 18:00 and 06:00 hours. Future SAR missions, like NiSAR and ROSE-L, are likely to be in similar orbits (Rosen et al., 2017; Pierdicca et al., 2019). Daily patterns in SCW should be taken into consideration when choosing to retrieve biophysical parameters from ascending or descending passes, or by combining data from both. Further research exploring the influence of frequency and viewing geometry is strongly recommended to support agricultural applications using data from these and other current and future SAR missions.

Results presented here show that the VOD estimate in the presence of SCW was higher than those estimated in its absence. In some sense, it is acceptable to say that the higher values of VOD from wet vegetation indicate a reduced sensitivity to soil moisture. However, this reduced sensitivity is not entirely attributable to the attenuation. It is hypothesized that the presence of water on the canopy may be leading to an increase in direct scattering from the vegetation, which is also reducing the signal that reaches the soil surface. The influence of SCW on multiple scattering, and how it might affect sensitivity to soil moisture is entirely unknown. This suggests that if VOD is to be used as a proxy for internal vegetation water content, backscatter values affected by SCW should not be included in the VOD estimate. In areas with strong daily cycles in dew or interception, it would be prudent to limit the estimation of VOD to satellite radar acquisitions at overpass times less likely to be affected by

SCW.

The conclusions drawn in this study are based on experimental data collected in a field experiment of limited duration, with a single crop type. Interestingly, similar conclusions were drawn in a recent study using VOD obtained from satellite passive microwave remote sensing, suggesting that the outcomes of this study are relevant for a wider range of cover types. Xu et al. (2021) used VOD data derived from X-band (10.7 GHz) measurements by the Advanced Microwave Scanning Radiometer for the Earth Observing System (AMSR-E) in combination with a terrestrial biosphere model in order to evaluate the relationship between canopy water content (CWC) and leaf surface water (LW_s) due to dew formation and rainfall interception with VOD at four tropical forest and savanna sites in Brazil. They found that LW_s accounts for >50% of diurnal variation in CWC at all four of the study sites that could make a large contribution to diurnal variation in CWC and AMSR-E VOD signals over tropical forests. Additional studies, over multiple locations, crop and land cover types are essential to characterize the impact of surface canopy water on retrievals of soil and vegetation states more generally from both active and passive microwave remote sensing.

All of the above point to an urgent need for an improved understanding of microwave interactions with vegetation in the presence of SCW. Additional experiments are strongly recommended to examine the influence of SCW over a wider range of vegetation. The capacity of various crops to store water will depend on their structure and geometry (e.g. narrow-leaved or broad-leaved etc.). These data are needed to understand how droplets or a film of water on the vegetation influences microwave interactions with the vegetation and soil. Inclusion of SCW in radiative transfer models of vegetated surfaces is essential to account for its influence in retrieval of soil and vegetation states. Furthermore, the potential to observe and retrieve SCW using radar remote sensing offers many new opportunities in the context of hydrology (Allen et al., 2020), and plant physiology (Dawson and Goldsmith, 2018).

CRediT author statement

S. Khabbazan: Conceptualization; Methodology; Formal analysis; Visualization; Writing - original draft; Writing - review & edit

S. Steele-Dunne: Conceptualization; Methodology; Writing - original draft; Supervision; Project administration; Investigation; Resources; Writing - review & edit

P. Vermunt: Visualization; Writing - review & edit

J. Judge: Methodology; Resources; Investigation; Writing - review & edit

M. Vreugdenhil: Methodology; Writing - original draft; Writing - review & edit

G. Gao: Software.

Declaration of Competing Interest

The authors declare that they have no known competing financial interests or personal relationships that could have appeared to influence the work reported in this paper.

Acknowledgments

This project was supported by Vidi Grant 14126 from the Dutch Technology Foundation TTW, which is part of The Netherlands Organisation for Scientific Research (NWO), and partly funded by the Ministry of Economic Affairs. The experiment was made possible by infrastructural and technical support from the Agr. and Biol. Eng. Dept. and PSREU at the University of Florida. The authors would like to thank Daniel Preston and Patrick Rush for their technical support, Eduardo Carrascal for data collection and processing, James Boyer and his team for their on-farm logistical support, and Roger DeRoo for useful insights about the UF-LARS system. We also appreciate the efforts of the anonymous reviewers and the editor.

References

Allen, C., Ulaby, F., 1984. Characterization of the Microwave Extinction Properties of Vegetation Canopies. Radiation Laboratory, Dept. of Electrical Engineering and Computer Science, The University of Michigan, Ann Arbor, MI, p. 48109.

Allen, S.T., Aubrey, D.P., Bader, M.Y., Coenders-Gerrits, M., Friesen, J., Gutmann, E.D., Guillemette, F., Jiménez-Rodríguez, C., Keim, R.F., Klamerus-Iwan, A., et al., 2020. Key questions on the evaporation and transport of intercepted precipitation. Precipitation Partitioning by Vegetation. Springer, Cham, pp. 269–280.

Attema, E.P.W., Ulaby, F.T., 1978. Vegetation modeled as a water cloud. Radio Sci. 13, 357–364. https://doi.org/10.1029/RS013i002p00357.

Barrett, B., Dwyer, E., Whelan, P., 2009. Soil moisture retrieval from active spaceborne microwave observations: an evaluation of current techniques. Rem. Sens. 1, 210–242. https://doi.org/10.3390/rs1030210.

Bindlish, R., Barros, A.P., 2001. Parameterization of vegetation backscatter in radar-based, soil moisture estimation. Rem. Sens. Environ. 76, 130–137. https://doi.org/10.1016/S0034-4257(00)00200-5.

Black, R.J., 1993. Florida climate data. CiteSeer, University of Florida Cooperative Extension Service, Institute of Food and Agriculture Sciences, EDIS.

Bongiovanni, T., Liu, P.W., Nagarajan, K., Preston, D., Rush, P., van Emmerik, T.H., Terwilleger, R., Monsivais-Huertero, A., Judge, J., Steele-Dunne, S., et al., 2015. Field Observations during the Eleventh Microwave Water and Energy Balance Experiment (MicroWEX-11): from April 25, 2012, through December 6. Agricultural and Biological Engineering Department, UF/IFAS Extension.

Bracaglia, M., Ferrazzoli, P., Guerriero, L., 1995. A fully polarimetric multiple scattering model for crops. Rem. Sens. Environ. 54, 170–179. https://doi.org/10.1016/0034-4257(95)00151-4.

Brakke, T.W., Kanemasu, E.T., Steiner, J.L., Ulaby, F.T., Wilson, E., 1981. Microwave radar response to canopy moisture, leaf-area index, and dry weight of wheat, corn, and sorghum. Rem. Sens. Environ. 11, 207–220.

Brancato, V., Liebisch, F., Hajnsek, I., 2017. Impact of plant surface moisture on differential interferometric observables: a controlled electromagnetic experiment. IEEE Trans. GeoSci. Rem. Sens. 55, 3949–3964.

Brisco, B., Brown, R.J., Hirose, T., McNairn, H., Staenz, K., 1998. Precision agriculture and the role of remote sensing: a review. Can. J. Rem. Sens. 24, 315–327. https://doi.org/10.1080/07038992.1998.10855254.

Bush, T.F., Ulaby, F.T., 1975. Fading characteristics of panchromatic radar backscatter from selected agricultural targets. IEEE Trans. Geosci. Electron. 13, 149–157.

Chang, Q., 2020. Mapping Shrub Biomass, Leaf Area Index and Rainfall Interception Capacities in the Arctic Tundra Using L-band SAR. Ph.D. thesis. University of Guelph.

Dawson, T.E., Goldsmith, G.R., 2018. The value of wet leaves. New Phytol. 219, 1156–1169.

Della Vecchia, A., Ferrazzoli, P., Guerriero, L., Blaes, X., Defourny, P., Dente, L., Mattia, F., Satalino, G., Strozzi, T., Wegmuller, U., 2006. Influence of geometrical factors on crop backscattering at c-band. IEEE Trans. GeoSci. Rem. Sens. 44, 778–790.

Dzikiti, S., Verreynne, J., Stuckens, J., Strever, A., Verstraeten, W., Swennen, R., Coppin, P., 2010. Determining the water status of Satsuma mandarin trees [Citrus Unshiu Marcovitch] using spectral indices and by combining hyperspectral and physiological data. Agric. Forest Meteorol. 150, 369–379. https://doi.org/10.1016/j.agrformet.2009.12.005. http://www.sciencedirect.com/science/article/pii/S0168192309002913.

El Hajj, M., Baghdadi, N., Bazzi, H., Zribi, M., 2018. Penetration analysis of SAR signals in the C and L bands for wheat, maize, and grasslands. Rem. Sens. 11, 31. https://doi.org/10.3390/rs11010031.

El Hajj, M., Baghdadi, N., Wigneron, J.P., Zribi, M., Albergel, C., Calvet, J.C., Fayad, I., 2019. First vegetation optical depth mapping from Sentinel-1 C-band SAR data over crop fields. Rem. Sens. 11, 2769. https://doi.org/10.3390/rs11232769.

Ferrazzoli, P., Paloscia, S., Pampaloni, P., Schiavon, G., Solimini, D., Coppo, P., 1992. Sensitivity of microwave measurements to vegetation biomass and soil moisture content: a case study. IEEE Trans. GeoSci. Rem. Sens. 30, 750–756. https://doi.org/10.1109/36.158869.

Fieuzal, R., Baup, F., Marais-Sicre, C., 2012. Sensitivity of TerraSAR-X, RADARSAT-2 and ALOS satellite radar data to crop variables. In: 2012 IEEE International Geoscience and Remote Sensing Symposium. IEEE, pp. 3740–3743. https://doi.org/10.1109/IGARSS.2012.6350504.

Frappart, F., Wigneron, J.P., Li, X., Liu, X., Al-Yaari, A., Fan, L., Wang, M., Moisy, C., Le Masson, E., Lafkih, Z.A., et al., 2020. Global monitoring of the vegetation dynamics from the Vegetation Optical Depth (VOD): a review. Rem. Sens. 12, 2915.

Gao, S., Niu, Z., Huang, N., Hou, X., 2013. Estimating the leaf area index, height and biomass of maize using HJ-1 and RADARSAT-2. Int. J. Appl. Earth Obs. Geoinfo. 24, 1–8. https://doi.org/10.1016/j.jag.2013.02.002.

Gillespie, T., Brisco, B., Brown, R., Sofko, G., 1990. Radar detection of a dew event in wheat. Rem. Sens. Environ. 33, 151–156. https://doi.org/10.1016/0034-4257(90)90026-I.

Haldar, D., Dave, V., Misra, A., Bhattacharya, B., 2020. Radar vegetation index for assessing cotton crop condition using risat-1 data. Geocarto Int. 35, 364–375.

Han, D., Yang, H., Yang, G., Qiu, C., 2017. Monitoring model of corn lodging based on Sentinel-1 radar image. In: 2017 SAR in Big Data Era: Models, Methods and Applications (BIGSARDATA). IEEE, pp. 1–5. https://doi.org/10.1109/BIGSARDATA.2017.8124928.

Herold, M., Pathe, C., Schmullius, C.C., 2001. The effect of free vegetation water on the multi-frequency and polarimetric radar backscatter – first results from the TerraDew 2000 campaign. In: IGARSS 2001. Scanning the Present and Resolving the Future. Proceedings. IEEE 2001 International Geoscience and Remote Sensing Symposium

(Cat. No.01CH37217), pp. 2445–2447. https://doi.org/10.1109/IGARSS.2001.978030 vol.5.
Hornbuckle, B.K., England, A.W., Anderson, M.C., Viner, B.J., 2006. The effect of free water in a maize canopy on microwave emission at 1.4 GHz. Agri. Forest Meteorol. 138, 180–191. https://doi.org/10.1016/j.agrformet.2006.05.003.
Hornbuckle, B.K., Rowlandson, T.L., Russell, E., Kaleita, A., Logsdon, S., Kruger, A., Yueh, S., De Roo, R.D., 2010. How does dew affect L-band backscatter? analysis of PALS data at the Iowa validation site and implications for SMAP. In: 2010 IEEE International Geoscience and Remote Sensing Symposium. IEEE, pp. 4835–4838.
Hosseini, M., McNairn, H., Merzouki, A., Pacheco, A., 2015. Estimation of Leaf Area Index (LAI) in corn and soybeans using multi-polarization C- and L-band radar data. Rem. Sens. Environ. 170, 77–89. https://doi.org/10.1016/j.rse.2015.09.002.
Huang, Y., Walker, J.P., Gao, Y., Wu, X., Monerris, A., 2016. Estimation of vegetation water content from the radar vegetation index at L-band. IEEE Trans. GeoSci. Rem. Sens. 54, 981–989. https://doi.org/10.1109/TGRS.2015.2471803.
Inoue, Y., Kurosu, T., Maeno, H., Uratsuka, S., Kozu, T., Dabrowska-Zielinska, K., Qi, J., 2002. Season-long daily measurements of multifrequency (Ka, Ku, X, C, and L) and full-polarization backscatter signatures over paddy rice field and their relationship with biological variables. Rem. Sens. Environ. 81, 194–204. https://doi.org/10.1016/S0034-4257(01)00343-1.
Jia, M., Tong, L., Zhang, Y., Chen, Y., 2013. Multitemporal radar backscattering measurement of wheat fields using multifrequency (L, S, C, and X) and full-polarization. Radio Sci. 48, 471–481. https://doi.org/10.1002/rds.20048.
Jiao, X., McNairn, H., Shang, J., Liu, J., 2010. The sensitivity of multi-frequency (X, C and L-band) radar backscatter signatures to bio-physical variables (LAI) over corn and soybean fields. In: ISPRS TC VII Symposium-100 Years ISPRS, pp. 317–325.
Jiao, X., McNairn, H., Shang, J., Pattey, E., Liu, J., Champagne, C., 2009. The sensitivity of RADARSAT-2 quad-polarization SAR data to crop LAI. https://doi.org/10.1117/12.825701, p. 74540O.
Kabela, E.D., Hornbuckle, B.K., Cosh, M.H., Anderson, M.C., Gleason, M.L., 2009. Dew frequency, duration, amount, and distribution in corn and soybean during SMEX05. Agric. Forest Meteorol. 149, 11–24. https://doi.org/10.1016/j.agrformet.2008.07.002.
Khabbazan, S., Vermunt, P., Steele-Dunne, S., Ratering Arntz, L., Marinetti, C., van der Valk, D., Iannini, L., Molijn, R., Westerdijk, K., van der Sande, C., 2019. Crop monitoring using Sentinel-1 data: a case study from the Netherlands. Rem. Sens. 11, 1887.
Kim, S.B., Huang, H., Liao, T.H., Colliander, A., 2018. Estimating vegetation water content and soil surface roughness using physical models of L-band radar scattering for soil moisture retrieval. Rem. Sens. 10, 556.
Kim, Y., Hong, S., Lee, K., Jackson, T., Bindlish, R., Jung, G., Jang, S., Na, Sangil, 2013a. Estimating wheat growth for radar vegetation indices. In: 2013 IEEE International Geoscience and Remote Sensing Symposium – IGARSS. IEEE, pp. 3219–3222. https://doi.org/10.1109/IGARSS.2013.6723512.
Kim, Y., Jackson, T., Bindlish, R., Hong, S., Jung, G., Lee, K., 2013b. Retrieval of wheat growth parameters with radar vegetation indices. IEEE Geosci. Rem. Sens. Lett. 11, 808–812.
Kim, Y., Jackson, T., Bindlish, R., Lee, H., Hong, S., 2011. Radar vegetation index for estimating the vegetation water content of rice and soybean. IEEE Geosci. Rem. Sens. Lett. 9, 564–568.
Kim, Y., van Zyl, J.J., 2009. A time-series approach to estimate soil moisture using polarimetric radar data. IEEE Trans. GeoSci. Rem. Sens. 47, 2519–2527.
Kim, Y.h., Hong, S.Y., Lee, H., 2008. Radar backscattering measurement of a paddy rice field using multi-frequency (L, C and X) and full-polarization. In: IGARSS 2008-2008 IEEE International Geoscience and Remote Sensing Symposium. IEEE. https://doi.org/10.1109/IGARSS.2008.4779781 pp. IV-553-IV-556.
Konings, A.G., Rao, K., Steele-Dunne, S.C., 2019. Macro to micro: microwave remote sensing of plant water content for physiology and ecology. New Phytolog. 223, 1166–1172.
Kross, A., McNairn, H., Lapen, D., Sunohara, M., Champagne, C., 2015. Assessment of RapidEye vegetation indices for estimation of leaf area index and biomass in corn and soybean crops. Int. J. Appl. Earth Obs. Geoinfo. 34, 235–248. https://doi.org/10.1016/j.jag.2014.08.002.
Kumar, P., Prasad, R., Gupta, D.K., Mishra, V.N., Vishwakarma, A.K., Yadav, V.P., Bala, R., Choudhary, A., Avtar, R., 2018. Estimation of winter wheat crop growth parameters using time series Sentinel-1A SAR data. Geocarto Int. 33, 942–956. https://doi.org/10.1080/10106049.2017.1316781.
Liao, C., Wang, J., Shang, J., Huang, X., Liu, J., Huffman, T., 2018. Sensitivity study of Radarsat-2 polarimetric SAR to crop height and fractional vegetation cover of corn and wheat. Int. J. Rem. Sens. 39, 1475–1490. https://doi.org/10.1080/01431161.2017.1407046.
Liu, P.W., Judge, J., DeRoo, R.D., England, A.W., Bongiovanni, T., Luke, A., 2016. Dominant backscattering mechanisms at L-band during dynamic soil moisture conditions for sandy soils. Rem Sens. Environ. 178, 104–112. https://doi.org/10.1016/j.rse.2016.02.062.
Ma, J., Huang, S., Li, J., Li, X., Song, X., Leng, P., Sun, Y., 2017. Estimating vegetation water content of corn and soybean using different polarization ratios based on L- and S-band radar data. IEEE Geosci. Rem. Sens. Lett. 14, 364–368. https://doi.org/10.1109/LGRS.2016.2643004.
Mahdianpari, M., Mohammadimanesh, F., McNairn, H., Davidson, A., Rezaee, M., Salehi, B., Homayouni, S., 2019. Mid-season crop classification using dual-, compact-, and full-polarization in preparation for the radarsat constellation mission (RCM). Rem. Sens. 11, 1582.
Mandal, D., Kumar, V., Ratha, D., Dey, S., Bhattacharya, A., Lopez-Sanchez, J.M., McNairn, H., Rao, Y.S., 2020a. Dual polarimetric radar vegetation index for crop growth monitoring using Sentinel-1 SAR data. Rem. Sens. Environ. 247, 111954. https://doi.org/10.1016/j.rse.2020.111954.
Mandal, D., Kumar, V., Ratha, D., Lopez-Sanchez, J.M., Bhattacharya, A., McNairn, H., Rao, Y., Ramana, K., 2020b. Assessment of rice growth conditions in a semi-arid region of India using the Generalized Radar Vegetation Index derived from RADARSAT-2 polarimetric SAR data. Rem Sens. Environ. 237, 111561.
McNairn, H., Brisco, B., 2004. The application of C-band polarimetric SAR for agriculture: a review. Can. J. Rem. Sens. 30, 525–542.
Meier, W., Bleiholder, H., Buhr, L., Feller, C., Hack, H., Heß, M., Lancashire, P.D., Schnock, U., Stauß, R., Van den Boom, T., Weber, E., Zwerger, P., 2009. The BBCH system to coding the phenological growth stages of plants – history and publications –. J. f“ur Kulturpflanzen 61, 41–52.
Group, METER., 2021a. ECHO EC-5 Moisture Sensor. https://www.metergroup.com/environment/products/ec-5-soil-moisture-sensor.
METER Group, 2021. PHYTOS 31 Dielectric Leaf Wetness Sensor. https://www.metergroup.com/environment/products/phytos-31-leaf-wetness-sensor.
Molijn, R.A., Iannini, L., López Dekker, P., Magalhães, P.S., Hanssen, R.F., 2018. Vegetation characterization through the use of precipitation-affected SAR signals. Rem. Sens. 10, 1647.
Molijn, R.A., Iannini, L., Mousivand, A., Hanssen, R.F., 2014. Analyzing C-band SAR polarimetric information for LAI and crop yield estimations. In: Remote Sensing for Agriculture, Ecosystems, and Hydrology XVI. International Society for Optics and Photonics, p. 92390V.
Monsivais-Huertero, A., Judge, J., 2011. Comparison of backscattering models at L-band for growing corn. IEEE Geosci. Rem. Sens. Lett. 8, 24–28. https://doi.org/10.1109/LGRS.2010.2050459.
Monsivais-Huertero, A., Liu, P.W., Judge, J., 2018. Phenology-based backscattering model for corn at L-band. IEEE Trans. GeoSci. Rem. Sens. 1–17. https://doi.org/10.1109/tgrs.2018.2803153.
Nagarajan, K., Liu, P.W., DeRoo, R., Judge, J., Akbar, R., Rush, P., Feagle, S., Preston, D., Terwilleger, R., 2013. Automated L-band radar system for sensing soil moisture at high temporal resolution. IEEE Geosci. Rem. Sens. Lett. 11, 504–508.
Ouaadi, N., Jarlan, L., Ezzahar, J., Khabba, S., Dantec, V.L., Rafi, Z., Zribi, M., Frison, P. L., 2020. Water stress detection over irrigated wheat crops in semi-arid areas using the diurnal differences of Sentinel-1 backscatter. In: 2020 Mediterranean and Middle-East Geoscience and Remote Sensing Symposium (M2GARSS). IEEE, pp. 306–309. https://doi.org/10.1109/M2GARSS47143.2020.9105171.
Paloscia, S., Pampaloni, P., 1992. Microwave vegetation indexes for detecting biomass and water conditions of agricultural crops. Rem Sens. Environ. 40, 15–26. https://doi.org/10.1016/0034-4257(92)90123-2.
Peel, M.C., Finlayson, B.L., McMahon, T.A., 2007. Updated world map of the K” oppen-Geiger climate classification. Hydrol. Earth Syst. Sci. 11, 1633–1644. https://doi.org/10.5194/hess-11-1633-2007.
Penuelas, J., Filella, I., Biel, C., Serrano, L., Save, R., 1993. The reflectance at the 950-970 nm region as an indicator of plant water status. Int. J. Rem. Sens. 14, 1887–1905. https://doi.org/10.1080/01431169308954010.
Pierdicca, N., Davidson, M., Chini, M., Dierking, W., Djavidnia, S., Haarpaintner, J., Hajduch, G., Laurin, G.V., Lavalle, M., López-Martínez, C., et al., 2019. The copernicus L-band SAR mission ROSE-L (Radar Observing System for Europe) (conference presentation). Active and Passive Microwave Remote Sensing for Environmental Monitoring III. International Society for Optics and Photonics, Strasbourg, France, p. 111540E.
Riedel, T., Pathe, C., Thiel, C., Herold, M., Schmullius, C., 2002. Systematic investigation on the effect of dew and interception on multifrequency and multipolarimetric radar backscatter signals. In: Wilson, A., Quegan, S. (Eds.), Retrieval of Bio- and Geo-Physical Parameters from SAR Data for Land Applications, pp. 99–104.
Rosen, P.A., Kim, Y., Kumar, R., Misra, T., Bhan, R., Sagi, V.R., 2017. Global persistent SAR sampling with the NASA-ISRO SAR (NISAR) mission. In: 2017 IEEE Radar Conference (RadarConf). IEEE, Seattle, WA, USA, pp. 0410–0414.
Saatchi, S.S., van Zyl, J.J., Asrar, G., 1995. Estimation of canopy water content in konza prairie grasslands using synthetic aperture radar measurements during fife. J. Geophys. Res.: Atmos. 100, 25481–25496.
Sarabandi, K., Ulaby, F.T., 1990. A convenient technique for polarimetric calibration of single-antenna radar systems. IEEE Trans. GeoSci. Rem. Sens. 28, 1022–1033.
Sharma, A., Lang, R.H., Kurum, M., O'Neill, P.E., Cosh, M.H., 2020. L-band radar experiment and modeling of a corn canopy over a full growing season. IEEE Trans. GeoSci. Rem. Sens. 58 (8), 5821–5835.
Slatyer, R.O., Markus, D.K., 1968. Plant–water relationships. Soil Sci. 106, 478.
Srivastava, P.K., O'Neill, P., Cosh, M., Lang, R., Joseph, A., 2015. Evaluation of radar vegetation indices for vegetation water content estimation using data from a ground-based SMAP simulator. In: 2015 IEEE International Geoscience and Remote Sensing Symposium (IGARSS). IEEE, Milan, Italy, pp. 1296–1299.
Steele-Dunne, S.C., Hahn, S., Wagner, W., Vreugdenhil, M., 2019. Investigating vegetation water dynamics and drought using Metop ASCAT over the North American Grasslands. Rem. Sens. Environ. 224, 219–235. https://doi.org/10.1016/j.rse.2019.01.004.
Steele-Dunne, S.C., McNairn, H., Monsivais-Huertero, A., Judge, J., Liu, P.W., Papathanassiou, K., 2017. Radar remote sensing of agricultural canopies: a review. IEEE J. Select. Top. Appl. Earth Obs. Rem. Sens. 10, 2249–2273. https://doi.org/10.1109/JSTARS.2016.2639043.
Szigarski, C., Jagdhuber, T., Baur, M., Thiel, C., Parrens, M., Wigneron, J.P., Piles, M., Entekhabi, D., 2018. Analysis of the radar vegetation index and potential improvements. Rem. Sens. 10, 1776.
Thenkabail, P.S., Lyon, J.G., 2016. Hyperspectral Remote Sensing of Vegetation. CRC Press, United state.

Tucker, C.J., 1980. Remote sensing of leaf water content in the near infrared. Rem Sens. Environ. 10, 23–32.

Ulaby, F.T., Sarabandi, K., McDONALD, K., Whitt, M., Dobson, M.C., 1990. Michigan microwave canopy scattering model. Int. J. Rem. Sens. 11, 1223–1253. https://doi.org/10.1080/01431169008955090.

Veloso, A., Mermoz, S., Bouvet, A., Le Toan, T., Planells, M., Dejoux, J.F., Ceschia, E., 2017. Understanding the temporal behavior of crops using Sentinel-1 and Sentinel-2-like data for agricultural applications. Rem. Sens. Environ. 199, 415–426.

Vermunt, P.C., Khabbazan, S., Steele-Dunne, S.C., Judge, J., Monsivais-Huertero, A., Guerriero, L., Liu, P.W., 2020. Response of subdaily L-band backscatter to internal and surface canopy water dynamics. IEEE Trans. GeoSci. Rem. Sens. 1–16. https://doi.org/10.1109/TGRS.2020.3035881.

Vreugdenhil, M., Dorigo, W.A., Wagner, W., De Jeu, R.A., Hahn, S., Van Marle, M.J., 2016. Analyzing the vegetation parameterization in the TU-Wien ASCAT soil moisture retrieval. IEEE Trans. Geosci. Rem. Sens. 54, 3513–3531.

Vreugdenhil, M., Wagner, W., Bauer-Marschallinger, B., Pfeil, I., Teubner, I., Rüdiger, C., Strauss, P., 2018. Sensitivity of Sentinel-1 backscatter to vegetation dynamics: An Austrian case study. Rem. Sens. 10, 1396.

Wagner, W., Lemoine, G., Rott, H., 1999. A method for estimating soil moisture from ers scatterometer and soil data. Rem. Sens. Environ. 70, 191–207.

Wood, D., McNairn, H., Brown, R.J., Dixon, R.G., 2002. The Effect of Dew on the Use of Radarsat-1 for Crop Monitoring: Choosing Between Ascending and descending orbits., a 80. https://doi.org/10.4095/219754.

Xu, X., Konings, A.G., Longo, M., Feldman, A., Xu, L., Saatchi, S., Wu, D., Wu, J., Moorcroft, P., 2021. Leaf surface Water, not Plant Water Stress, Drives Diurnal Variation in Tropical Forest Canopy Water Content. New Phytologist, Lancaster University.